Two-loop leading colour helicity amplitudes for W+/-γ + j production at the LHC

(Article begins on next page)

Two-loop leading colour helicity amplitudes for $W^{\pm}\gamma + j$ production at the LHC

Simon Badger,[a] Heribertus Bayu Hartanto,[b] Jakub Kryś,[a,c] Simone Zoia[a]

[a]*Dipartimento di Fisica and Arnold-Regge Center, Università di Torino, and INFN, Sezione di Torino, Via P. Giuria 1, I-10125 Torino, Italy*

[b]*Cavendish Laboratory, University of Cambridge, Cambridge CB3 0HE, United Kingdom*

[c]*Institute for Particle Physics Phenomenology, Department of Physics, Durham University, Durham DH1 3LE, United Kingdom*

E-mail: simondavid.badger@unito,it, hbhartanto@hep.phy.cam.ac.uk, jakubmarcin.krys@unito.it, simone.zoia@unito.it

ABSTRACT: We present the two-loop leading colour QCD helicity amplitudes for the process $pp \to W(\to l\nu)\gamma + j$. We implement a complete reduction of the amplitudes, including the leptonic decay of the W-boson, using finite field arithmetic, and extract the analytic finite remainders using a recently identified basis of special functions. Simplified analytic expressions are obtained after considering permutations of a rational kinematic parametrisation and multivariate partial fractioning. We demonstrate efficient numerical evaluation of the two-loop colour and helicity summed finite remainders for physical kinematics, and hence the suitability for phenomenological applications.

Contents

1 Introduction

High-precision theoretical predictions are a high priority for the current experiments at the Large Hadron Collider (LHC). Processes with a pair of electroweak vector bosons ($W^{\pm}, Z, \gamma$) offer a wide range of observables which can test electroweak couplings and probe the Higgs sector of the Standard Model. In particular, the production of a W boson in association with a photon ($pp \rightarrow W\gamma$) is one of the processes observed at the LHC with relatively large cross sections where clean signatures can be acquired when the W boson decays leptonically. $W\gamma$ production enables direct access to the $WW\gamma$ triple gauge boson coupling, which can be modified in certain new physics scenarios. Both ATLAS and CMS experiments have measured the $W\gamma$ process [1–6] and set the limit on the anomalous $WW\gamma$ coupling.

Predictions for $pp \rightarrow W^{\pm}\gamma$ are available through to next-to-next-to-leading order (NNLO) in QCD [7–9] and NLO in the electroweak (EW) coupling [10, 11] as well as combined NNLO in QCD and NLO in EW [12]. The colourless final state makes the process well suited for the q_T [13] and N-jettiness [14, 15] subtraction methods as implemented within the MATRIX [16] and MCFM [17] Monte Carlo event generators, respectively. Resummed predictions including parton shower effects are now available [18], making this one of the most precisely known theoretical predictions. Experimental measurements are constantly improving and provide rich opportunities for precision SM tests [6, 19]. In order to suppress different types of backgrounds in the experimental analysis, it is a common practice to divide the measurement according to the jet multiplicities, i.e. $W\gamma+0$ jet, $W\gamma+1$ jet, $W\gamma+2$ jets, etc. Increasing the precision of the theoretical predictions for each of the jet bins amounts to computing higher order corrections to $W\gamma$ production in association with additional jets.

In this article we compute the two-loop helicity amplitudes for the process $pp \rightarrow W^{\pm}(\rightarrow l^{\pm}\nu)\gamma + j$ for the first time. The amplitude-level ingredients we provide will give useful information for future precision measurements of anomalous couplings and potentially for complete global fits of the Standard Model Effective Theory (SMEFT). A fully differential computation of $W\gamma+j$ at NNLO in QCD would also open up the possibility of N³LO QCD predictions for $W\gamma$ production.

The process has already been well studied at NLO in QCD [20], including the anomalous couplings [21], and is easily within the reach of standard automated tools including electroweak corrections. Compact analytic formulae at one loop have been obtained recently [9].

Recent years have seen tremendous progress in the analytic computation of two-loop amplitudes for processes involving five massless particles [22–41]. The methods are now reaching maturity also for two-loop five-particle amplitudes with an external off-shell leg, with the first sets of analytic helicity amplitudes in the planar limit appearing over the last 12 months [42–44]. This progress has been made possible by the classification of the special functions appearing in the finite remainders through the differential equations they satisfy [45–51]. Furthermore, finite-field arithmetic for scattering amplitudes [52–54] allows us to avoid the large intermediate expressions and provides efficient solutions to large systems of integration-by-parts integral identities [55–57], which are the main bottlenecks in the analytic computation of multi-loop scattering amplitudes.

Our paper is organised as follows. In Section 2 we describe the structure of the amplitudes for $pp \rightarrow W\gamma j$ up to two loops, paying particular attention to the description of the decay of the W boson. In Section 3 we describe the finite field reduction setup used to extract the finite remainders, and propose an approach to simplify dramatically the analytic expressions of the latter based on a systematic search of a better parameterisation of the kinematics in terms of momentum-twistor variables. We describe a number of validation tests that have been performed on our results in Section 4, and then present some numerical results for the colour and helicity summed finite remainders in Section 5. We present our conclusions and outlook for the future in Section 6. Complete analytic expressions are provided in the associated ancillary files on the arXiv. In addition, we include appendices
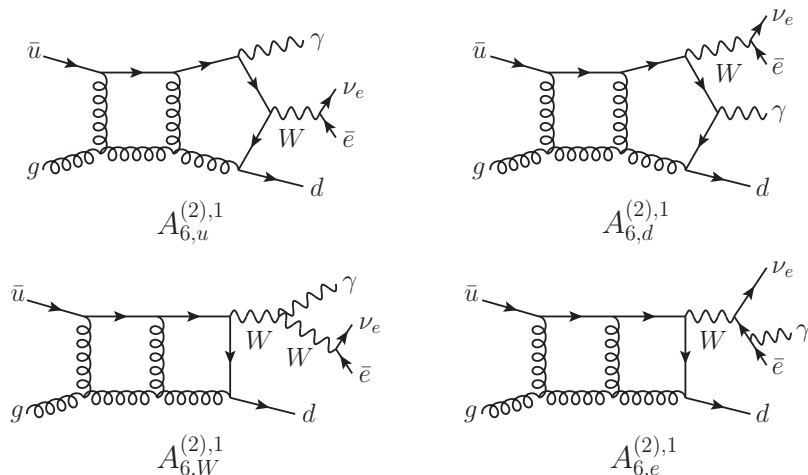
Figure 1: Sample two-loop Feynman diagrams for $W^+\gamma j$ production.

describing the details of the renormalisation constants, and giving explicit one-loop results to facilitate future cross-checks.

2 Structure of the Amplitudes

We compute the two-loop amplitudes for the production of a W^+ boson in association with a photon and a jet at hadron colliders, where the W^+ boson decays to a positron and an electron neutrino ($pp \to \nu_e e^+ \gamma j$), in the leading colour approximation,

$$0 \to \gamma(p_1, h_1) + \bar{u}(p_2, h_2) + g(p_3, h_3) + d(p_4, h_4) + \nu_e(p_5, h_5) + e^+(p_6, h_6) \,. \qquad (2.1)$$

For simplicity we denote this process as $W^+\gamma j$ production henceforth. Sample two-loop Feynman diagrams contributing at leading colour are shown in Figures 1 and 2. The colour decomposition of the $W^+\gamma j$ L-loop amplitude is given by

$$\mathcal{A}_6^{(L)}(1_\gamma, 2_{\bar{u}}, 3_g, 4_d, 5_\nu, 6_{\bar{e}}) = \sqrt{2} e g_W^2 g_s \, n^L \, (T^{a_3})_{i_4}^{\bar{i}_2} \, A_6^{(L)}(1_\gamma, 2_{\bar{u}}, 3_g, 4_d, 5_\nu, 6_{\bar{e}}) \,, \qquad (2.2)$$

where $n = m_\epsilon \alpha_s/(4\pi)$, $\alpha_s = g_s^2/(4\pi)$, $m_\epsilon = i(4\pi)^\epsilon e^{-\epsilon \gamma_E}$, $\epsilon = (4-d)/2$ is the dimensional regulator, and T^a are the generators of $SU(N_c)$ in the fundamental representation, normalised according to $\text{tr}(T^a T^b) = \delta^{ab}$. We denote by e, g_W and g_s the electron charge, the weak and the strong coupling constants, respectively. The $W^+\gamma j$ amplitude can be further decomposed according to the source of photon radiation,

$$
\begin{aligned}
A_6^{(L)} = & \left[Q_u A_{6,u}^{(L)} + Q_d A_{6,d}^{(L)} + \left(\sum_q Q_q \right) A_{6,q}^{(L)} \right] P(s_{56}) \\
& + (Q_u - Q_d) \left[A_{6,e}^{(L)} + A_{6,W}^{(L)} P(s_{56}) \right] P(s_{156}) \,,
\end{aligned}
\qquad (2.3)
$$

– 3 –
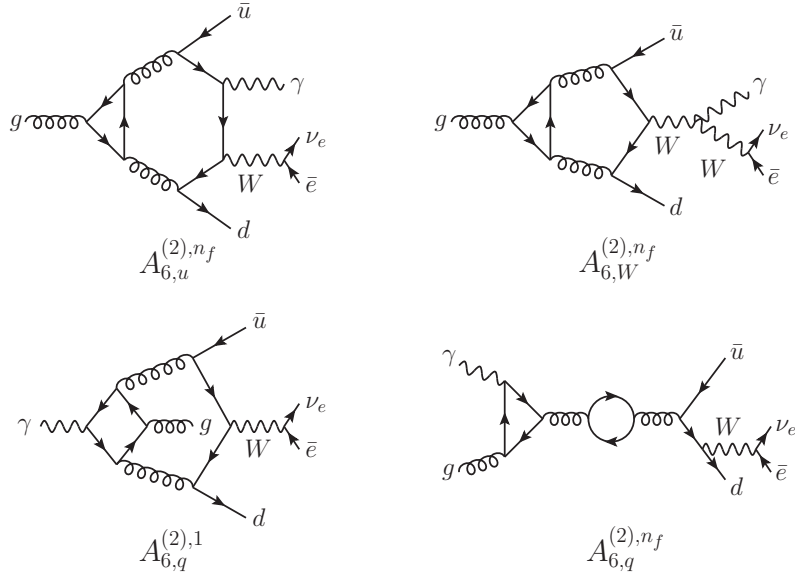
Figure 2: Sample two-loop Feynman diagrams for $W^+\gamma j$ production containing closed fermion loop. $A_{6,q}^{(2),n_f}$ vanishes due to Furry's theorem.

where $s_{ij} = (p_i + p_j)^2$ and $s_{ijk} = (p_i + p_j + p_k)^2$, Q_u and Q_d are the up- and down-quark charges respectively, the sum runs over the quark flavours q, while

$$P(s) = \frac{1}{s - M_W^2 + iM_W\Gamma_W} \, , \tag{2.4}$$

is the denominator factor of W boson propagator. M_W and Γ_W are the mass and decay width of the W boson, respectively. The sub-amplitudes $A_{6,i}^{(L)}$ in Eq. (2.3) are categorised as follows:

- $A_{6,u}^{(L)}$: the photon is radiated off the u quark;

- $A_{6,d}^{(L)}$: the photon is radiated off the d quark;

- $A_{6,W}^{(L)}$: the photon is radiated off the W boson;

- $A_{6,e}^{(L)}$: the photon is radiated off the positron;

- $A_{6,q}^{(L)}$: the photon is radiated off the internal quark loop.

We stress that the sub-amplitudes are not separately gauge invariant in the electroweak sector. Using the relation [9]

$$P(s_{56})P(s_{156}) = \frac{1}{s_{156} - s_{56}}\left[P(s_{56}) - P(s_{156})\right] \tag{2.5}$$

we can rewrite Eq. (2.3) as

$$A_6^{(L)} = Q_u \left[A_{6,u}^{(L)} + \frac{1}{s_{156} - s_{56}} A_{6,W}^{(L)} \right] P(s_{56}) + Q_d \left[A_{6,d}^{(L)} - \frac{1}{s_{156} - s_{56}} A_{6,W}^{(L)} \right] P(s_{56})$$

$$+ (Q_u - Q_d) \left[A_{6,e}^{(L)} - \frac{1}{s_{156} - s_{56}} A_{6,W}^{(L)} \right] P(s_{156}) + \left(\sum_q Q_q \right) A_{6,q}^{(L)} P(s_{56}) , \quad (2.6)$$

such that the combinations of sub-amplitudes in the square brackets and $A_{6,q}^{(L)}$ are the gauge invariant pieces. We further decompose the sub-amplitudes according to their closed fermion loop contributions. At leading colour we have

$$A_{6,i}^{(1)} = N_c A_{6,i}^{(1),1} ,$$
$$A_{6,i}^{(2)} = N_c^2 A_{6,i}^{(2),1} + N_c n_f A_{6,i}^{(2),n_f} , \quad (2.7)$$
$$A_{6,q}^{(2)} = N_c A_{6,q}^{(2),1} ,$$

where $i = u, d, W, e$, and n_f is the number of massless quark flavours running in the loop. We note that $A_{6,q}^{(L)}$ vanishes at tree level and one loop, while at two loops it includes non-planar contributions, and thus will not be considered in this work.

The coupling of the W boson to fermions involves vector and axial-vector $(V - A)$ vertices in the form of $\gamma^\mu (1 - \gamma_5)/2$. The massless fermion pairs that are coupled to the W boson are connected to the external states and the $V - A$ coupling fixes the helicity of the fermion pairs. Therefore we only need to take into account the vector coupling of the W boson to fermions when computing the helicity amplitudes. The contributing helicity configurations are

$$A_6^{(L)}(1_\gamma^\pm, 2_{\bar{u}}^+, 3_g^\pm, 4_d^-, 5_\nu^-, 6_{\bar{e}}^+) .$$

We choose $+++--+$ and $-++--+$ as the independent helicity configurations and focus on them. We obtain the amplitudes in the other helicity configurations from the independent ones by suitably permuting the external momenta and conjugating space-time parity.

The sub-amplitudes $A_{6,u}^{(L)}$ and $A_{6,d}^{(L)}$ are related by

$$A_{6,u}^{(L)}(1_\gamma^{h_1}, 2_{\bar{u}}^+, 3_g^{h_3}, 4_d^-, 5_\nu^{h_5}, 6_{\bar{e}}^{h_6}) = A_{6,d}^{(L)}(1_\gamma^{h_1}, 4_{\bar{u}}^-, 3_g^{h_3}, 2_d^+, 5_\nu^{h_5}, 6_{\bar{e}}^{h_6}) . \quad (2.8)$$

As a result, we can limit ourselves to computing the $A_{6,d}^{(L)}$ sub-amplitudes with the following helicity configurations,

$$A_{6,d}^{(L)}(1_\gamma^\pm, 2_{\bar{u}}^\pm, 3_g^\pm, 4_d^\mp, 5_\nu^-, 6_{\bar{e}}^+) .$$

The independent helicity amplitudes for $A_{6,u}^{(L)}$ are then obtained through

$$A_{6,u}^{(L)}(1_\gamma^\pm, 2_{\bar{u}}^+, 3_g^+, 4_d^-, 5_\nu^-, 6_{\bar{e}}^+) = A_{6,d}^{(L)}(1_\gamma^\pm, 4_{\bar{u}}^-, 3_g^+, 2_d^+, 5_\nu^-, 6_{\bar{e}}^+) . \quad (2.9)$$

The pole structure of the unrenormalised $W^+ \gamma j$ amplitudes in the 't Hooft-Veltman (tHV) scheme at one and two loops is given by [58–61]

$$P_6^{(1)} = 2I_1(\epsilon) + \frac{\beta_0}{2\epsilon}, \quad (2.10)$$

$$P_6^{(2)} = 2I_1(\epsilon) \left(\hat{A}_6^{(1)} - \frac{\beta_0}{2\epsilon} \right) + 4I_2(\epsilon) + \frac{3\beta_0}{2\epsilon} \hat{A}_6^{(1)} - \frac{3\beta_0^2}{8\epsilon^2} + \frac{\beta_1}{4\epsilon} , \quad (2.11)$$

where $\hat{A}_6^{(1)}$ is the unrenormalised one-loop amplitude divided by the tree-level amplitude. The $I_2(\epsilon)$ operator is given by

$$I_2(\epsilon) = -\frac{1}{2}I_1(\epsilon)\left[I_1(\epsilon) + \frac{\beta_0}{\epsilon}\right] + \frac{N(\epsilon)}{N(2\epsilon)}\left[\frac{\beta_0}{2\epsilon} + \frac{\gamma_1^{\text{cusp}}}{8}\right]I_1(2\epsilon) + H^{(2)}(\epsilon)\,, \qquad (2.12)$$

while the $I_1(\epsilon)$ operator is given at leading colour by

$$I_1(\epsilon) = -N_c\frac{N(\epsilon)}{2}\left(\frac{1}{\epsilon^2} + \frac{3}{4\epsilon} + \frac{\beta_0}{4N_c\epsilon}\right)\left[(-s_{23})^{-\epsilon} + (-s_{34})^{-\epsilon}\right]\,, \qquad (2.13)$$

where $N(\epsilon) = e^{\epsilon\gamma_E}/\Gamma(1-\epsilon)$ and

$$H^{(2)}(\epsilon) = \frac{1}{16\epsilon}\left\{(2\gamma_1^q + \gamma_1^g) - \gamma_1^{\text{cusp}}\left(\frac{\gamma_0^q}{2} + \frac{\gamma_0^g}{4}\right) + \frac{\pi^2}{8}\beta_0\gamma_0^{\text{cusp}}\left(C_F + \frac{C_A}{2}\right)\right\}\,. \qquad (2.14)$$

The β function coefficients and anomalous dimensions are tabulated in Appendix A. We stress that the pole terms in Eqs. (2.10) and (2.11) include both the ultraviolet and infrared singularities. We then extract the L-loop partial finite remainder by subtracting the poles $P_6^{(L)}$ from the unrenormalised partial amplitude $A_6^{(L)}$ and sending ϵ to 0,

$$F_6^{(L)} = \lim_{\epsilon\to 0}\left[A_6^{(L)} - P_6^{(L)}A_6^{(0)}\right]\,. \qquad (2.15)$$

The finite remainder $F_6^{(L)}$ follows the same decomposition as the unrenormalised partial amplitude $A_6^{(L)}$ (see Eqs. (2.3) and (2.7)),

$$F_6^{(L)} = \left[Q_u F_{6,u}^{(L)} + Q_d F_{6,d}^{(L)}\right]P(s_{56}) + (Q_u - Q_d)\left[F_{6,e}^{(L)} + F_{6,W}^{(L)}P(s_{56})\right]P(s_{156})\,, \qquad (2.16)$$

with

$$\begin{aligned}
F_{6,i}^{(1)} &= N_c F_{6,i}^{(1),1} + n_f F_{6,i}^{(1),n_f}\,, \\
F_{6,i}^{(2)} &= N_c^2 F_{6,i}^{(2),1} + N_c n_f F_{6,i}^{(2),n_f} + n_f^2 F_{6,i}^{(2),n_f^2}\,,
\end{aligned} \qquad (2.17)$$

where $i = u, d, W, e$. We note that, although the bare sub-amplitudes $A_{6,i}^{(1),n_f}$ and $A_{6,i}^{(2),n_f^2}$ vanish, there are finite contributions to the finite remainders $F_{6,i}^{(1),n_f}$ and $F_{6,i}^{(2),n_f^2}$ from the UV renormalisation and IR subtraction terms specified in Eqs. (2.10) and (2.11). As discussed below Eqs. (2.7), we defer the computation of $F_{6,q}^{(2)}$, as it involves the non-planar integrals.

For the charge-conjugated process, i.e. $pp \to \bar{\nu}_e e^-\gamma j$, we consider the amplitudes for

$$0 \to \gamma(p_1, h_1) + \bar{d}(p_2, h_2) + g(p_3, h_3) + u(p_4, h_4) + e^-(p_5, h_5) + \bar{\nu}_e(p_6, h_6)\,,$$

which we denote by $W^-\gamma j$ production. The amplitudes for $W^-\gamma j$ production can be obtained from the $W^+\gamma j$ results through the following relation,

$$A_6^{(L)}(1_\gamma^{-h_1}, 2_{\bar{d}}^+, 3_g^{-h_3}, 4_u^-, 5_e^-, 6_{\bar{\nu}}^+) = \left[A_6^{(L)}(1_\gamma^{h_1}, 4_{\bar{u}}^+, 3_g^{h_3}, 2_{\bar{d}}^-, 6_{\bar{\nu}}^-, 5_{\bar{e}}^+)\right]_{\langle ij\rangle\leftrightarrow[ij]}\,. \qquad (2.18)$$

3 Amplitude Computation

In this section we describe the computation of the two-loop $W^+\gamma j$ amplitude in the leading colour approximation. To derive the analytic form of the amplitude we employ a framework that combines Feynman diagram input, the four-dimensional projector method [62, 63], integration-by-parts (IBP) reduction [55–57], Laurent expansion onto a basis of special function, numerical evaluations over finite fields, and analytic reconstruction techniques [52–54].

Instead of computing the loop amplitudes using the full six-particle kinematics, we detach the leptonic decay of the W boson from the amplitude and only compute the W-production amplitudes. For the $A_{6,u}^{(L)}$ and $A_{6,d}^{(L)}$ sub-amplitudes the W-production amplitude is a five-point amplitude with an off-shell leg (denoted by $A_{5,u/d}^{(L)\mu}$), while for the $A_{6,W}^{(L)}$ and $A_{6,e}^{(L)}$ sub-amplitudes the W-production amplitude is a four-point amplitude with an off-shell leg (denoted by $A_4^{(L)\mu}$),

$$A_{6,u/d}^{(L)}(p_1, p_2, p_3, p_4, p_5, p_6) = A_{5,u/d}^{(L)\mu}(p_1, p_2, p_3, p_4, p_W)\, L_{A,\mu}(p_5, p_6)\,, \tag{3.1}$$

$$A_{6,e/W}^{(L)}(p_1, p_2, p_3, p_4, p_5, p_6) = A_4^{(L)\mu}(p_2, p_3, p_4, \tilde{p}_W)\, L_{B,\mu}^{e/W}(p_1, p_5, p_6)\,, \tag{3.2}$$

where $p_W = p_5 + p_6$ and $\tilde{p}_W = p_1 + p_5 + p_6$, $L_{B,\mu}^e$ ($L_{B,\mu}^W$) is the decay current where the photon is emitted from the positron (W boson), while $L_{A,\mu}$ is simply the $W^+ \to \nu e^+$ decay current. The QCD corrections affect only the W-production amplitudes $A_{5,u/d}^{(L)\mu}$ and $A_4^{(L)\mu}$. We adopt the same decomposition for the finite remainders,

$$F_{6,u/d}^{(L)}(p_1, p_2, p_3, p_4, p_5, p_6) = F_{5,u/d}^{(L)\mu}(p_1, p_2, p_3, p_4, p_W)\, L_{A,\mu}(p_5, p_6)\,, \tag{3.3}$$

$$F_{6,e/W}^{(L)}(p_1, p_2, p_3, p_4, p_5, p_6) = F_4^{(L)\mu}(p_2, p_3, p_4, \tilde{p}_W)\, L_{B,\mu}^{e/W}(p_1, p_5, p_6)\,. \tag{3.4}$$

In the next subsections we discuss the computation of $F_{5,d}^{(L)\mu}$ and $F_4^{(L)\mu}$. We recall that $F_{6,u}^{(L)}$ can be obtained from $F_{6,d}^{(L)}$ through the amplitude-level relation given in Eq. (2.8), which we rewrite here for the finite remainders,

$$F_{6,u}^{(L)}(1_\gamma^{h_1}, 2_{\bar{u}}^+, 3_g^{h_3}, 4_d^-, 5_\nu^{h_5}, 6_{\bar{e}}^{h_6}) = F_{6,d}^{(L)}(1_\gamma^{h_1}, 4_{\bar{u}}^-, 3_g^{h_3}, 2_d^+, 5_\nu^{h_5}, 6_{\bar{e}}^{h_6})\,. \tag{3.5}$$

We begin by describing how we parameterise the kinematics. Next, we discuss how we decompose the W-production five- and four-particle amplitudes, in Sections 3.2 and 3.3 respectively, using the projector method. Section 3.4 is devoted to the finite-field setup which we use to reconstruct the analytic expressions of the finite remainders as linear combinations of rational coefficients and monomials of independent special functions. In Section 3.5 we present a strategy which allows us to simplify dramatically the expressions of the rational coefficients. Finally, in Section 3.6 we discuss how our analytic results for the minimal set of independent finite remainders can be used efficiently to evaluate numerically all the contributions to the squared finite remainder summed over helicity and colour.

3.1 Kinematics

In this section we describe the kinematics of the process $W^+\gamma j$ (2.1). All the external momenta p_i^μ are massless,

$$p_i^2 = 0 \quad \forall\, i = 1, \ldots, 6\,, \tag{3.6}$$

and taken to be outgoing, so that momentum conservation is

$$\sum_{i=1}^{6} p_i = 0\,. \tag{3.7}$$

We consider the external momenta p_i^μ to live in a four-dimensional Minkowski space. As a result there are eight independent scalar invariants, which we choose as

$$\vec{s}_6 = \{s_{12}, s_{23}, s_{34}, s_{45}, s_{56}, s_{16}, s_{123}, s_{234}\}\,. \tag{3.8}$$

It is also possible to form pseudo-scalar invariants by contracting the Levi-Civita symbol $\epsilon_{\mu\nu\rho\sigma}$ with any four external momenta. The six-particle kinematics is therefore fully determined by the scalar invariants $\vec{s}_6$ and by one pseudo-scalar invariant, which captures all the space-time parity information of the phase space. In analogy with the five-particle kinematics, we choose

$$\mathrm{tr}_5 = 4i\epsilon_{\mu\nu\rho\sigma}p_1^\mu p_2^\nu p_3^\rho p_4^\sigma\,. \tag{3.9}$$

The latter is related to the scalar invariants through

$$\mathrm{tr}_5^2 = \Delta_5 := \det\left(2p_i \cdot p_j\right)\big|_{i,j=1,\ldots,4}\,, \tag{3.10}$$

where the right-hand side is a degree-four polynomial in the scalar invariants.

Only a subset of these invariants are relevant for the computation of $A_{5,d}^{(L)\mu}$, which has five-point kinematics with an external massive particle. We choose the following independent five-point scalar invariants for computing $A_{5,d}^{(L)\mu}$,

$$\vec{s}_5 = \{s_{12}, s_{23}, s_{34}, s_{123}, s_{234}, s_{56}\}\,, \tag{3.11}$$

together with tr_5. Even fewer variables are relevant for $A_4^{(L)\mu}$. Since the latter has four-point kinematics with an external massive particle, no pseudo-scalar invariant can be formed and it is thus independent of tr_5. Moreover, it depends only on three of the scalar invariants in $\vec{s}_5$. Nonetheless, we view it as a function of $\vec{s}_5$ in order to have a homogeneous setup.

When attaching the W-boson decay currents ($L_{A,\mu}$ and $L_{B,\mu}^{e/W}$) to $A_{5,d}^{(L)\mu}$ and $A_4^{(L)\mu}$ (see Eqs. (3.1) and (3.2)) we find it convenient to describe the massless six-point kinematics using a parameterisation based on momentum twistors [64] (see e.g. Refs. [65, 66] for a thorough discussion of momentum twistors in this context). We adopt the following momentum-twistor parameterisation,

$$Z = \begin{pmatrix} 1 & 0 & y_1 & y_2 & y_3 & y_4 \\ 0 & 1 & 1 & 1 & 1 & 1 \\ 0 & 0 & 0 & \frac{x_5}{x_2} & x_6 & 1 \\ 0 & 0 & 1 & 1 & x_7 & 1 - \frac{x_8}{x_5} \end{pmatrix}, \tag{3.12}$$

where the columns give the four-component momentum twistors of the six external particles, and we used the short-hand notation $y_i = \sum_{j=1}^{i} \prod_{k=1}^{j} \frac{1}{x_k}$. The eight momentum-twistor variables x_i are related to the external momenta through

$$x_1 = s_{12}\,, \quad x_2 = -\frac{\mathrm{tr}_+(1234)}{s_{12}s_{34}}\,, \qquad x_3 = -\frac{\mathrm{tr}_+(1345)}{s_{45}s_{13}}\,, \qquad x_4 = -\frac{\mathrm{tr}_+(1456)}{s_{14}s_{56}}\,,$$
$$x_5 = \frac{s_{23}}{s_{12}}\,, \quad x_6 = -\frac{\mathrm{tr}_+(15(3+4)2)}{s_{12}s_{15}}\,, \quad x_7 = \frac{\mathrm{tr}_+(51(2+3)(2+3+4))}{s_{15}s_{23}}\,, \quad x_8 = \frac{s_{123}}{s_{12}}\,,$$
$$(3.13)$$

with $\mathrm{tr}_\pm(ij\cdots kl) = \mathrm{tr}((1\pm\gamma_5)\slashed{p}_i\slashed{p}_j\cdots\slashed{p}_k\slashed{p}_l)/2$. Note that the momentum-twistor variables x_i in general transform in a non-trivial way under space-time parity. We implement the action of parity on momentum-twistor expressions as a change of momentum-twistor variables which leave unchanged the scalar invariants and flips the sign of tr_5. The definition of the parity-flipped momentum-twistor variables can be obtained by trading tr_+ for tr_- in Eqs. (3.13).

3.2 Structure of the five-particle W-production amplitudes

We decompose the five-point W-production amplitude $A_{5,d}^{(L)\mu}$ using the external momenta (p_1, p_2, p_3, p_4) as the spanning basis,

$$A_{5,d}^{(L)\mu} = p_1^\mu a_1^{(L)} + p_2^\mu a_2^{(L)} + p_3^\mu a_3^{(L)} + p_4^\mu a_4^{(L)}\,. \tag{3.14}$$

The coefficients $a_i^{(L)}$ can be obtained by inverting the system of equations

$$a_i^{(L)} = \sum_{j=1}^{4} \left(\Delta^{-1}\right)_{ij} \tilde{A}_{5,j}^{(L)}\,, \tag{3.15}$$

where

$$\Delta_{ij} = p_i \cdot p_j\,, \tag{3.16}$$
$$\tilde{A}_{5,i}^{(L)} = p_i \cdot A_{5,d}^{(L)}\,. \tag{3.17}$$

The *contracted amplitudes* $\tilde{A}_{5,i}^{(L)}$ are computed by first generating the five-point process with an on-shell W boson, followed by replacing the W-boson polarisation vector by the four external momenta in the spanning basis, (p_1, p_2, p_3, p_4). We then apply tensor decomposition, taking into account the four-dimensional nature of the external states as proposed in Refs. [62, 63], to express each contracted amplitude $\tilde{A}_{5,i}^{(L)}$ as a linear combination of 8 independent tensor structures $\{T_j\}_{j=1}^{8}$,

$$\tilde{A}_{5,i}^{(L)} = \sum_{j=1}^{8} T_j \alpha_{i,j}^{(L)}\,, \tag{3.18}$$

where

$$T_1 = \bar{u}(p_4)\slashed{p}_1 v(p_2)\, p_2 \cdot \varepsilon(p_1, q_1)\, p_2 \cdot \varepsilon(p_3, q_3)\,,$$

$$T_2 = \bar{u}(p_4)\slashed{p}_1 v(p_2)\, p_2 \cdot \varepsilon(p_1, q_1)\, p_4 \cdot \varepsilon(p_3, q_3)\,,$$

$$T_3 = \bar{u}(p_4)\slashed{p}_1 v(p_2)\, p_4 \cdot \varepsilon(p_1, q_1)\, p_2 \cdot \varepsilon(p_3, q_3)\,,$$

$$T_4 = \bar{u}(p_4)\slashed{p}_1 v(p_2)\, p_4 \cdot \varepsilon(p_1, q_1)\, p_4 \cdot \varepsilon(p_3, q_3)\,, \qquad (3.19)$$

$$T_5 = \bar{u}(p_4)\slashed{p}_3 v(p_2)\, p_2 \cdot \varepsilon(p_1, q_1)\, p_2 \cdot \varepsilon(p_3, q_3)\,,$$

$$T_6 = \bar{u}(p_4)\slashed{p}_3 v(p_2)\, p_2 \cdot \varepsilon(p_1, q_1)\, p_4 \cdot \varepsilon(p_3, q_3)\,,$$

$$T_7 = \bar{u}(p_4)\slashed{p}_3 v(p_2)\, p_4 \cdot \varepsilon(p_1, q_1)\, p_2 \cdot \varepsilon(p_3, q_3)\,,$$

$$T_8 = \bar{u}(p_4)\slashed{p}_3 v(p_2)\, p_4 \cdot \varepsilon(p_1, q_1)\, p_4 \cdot \varepsilon(p_3, q_3)\,.$$

Here, q_1 and q_3 are arbitrary reference vectors for the photon and the gluon polarisation states, respectively. We set $q_1 = p_3$ and $q_3 = p_1$ throughout our computation. The tensor coefficients $\alpha_{i,j}^{(L)}$ can be obtained by

$$\alpha_{i,j}^{(L)} = \sum_{k=1}^{8} \left(\Theta^{-1}\right)_{jk} \sum_{\text{pol}} T_k^\dagger \tilde{A}_{5,i}^{(L)}\,, \qquad (3.20)$$

where

$$\Theta_{ij} = \sum_{\text{pol}} T_i^\dagger T_j\,, \qquad (3.21)$$

and the polarisation-vector sum for the photon and gluon is

$$\sum_{\text{pol}} \varepsilon_\mu^*(p_i, q_i)\varepsilon_\nu(p_i, q_i) = -g_{\mu\nu} + \frac{p_{i\mu}q_{i\nu} + q_{i\mu}p_{i\nu}}{p_i \cdot q_i}\,, \qquad i = 1, 3\,. \qquad (3.22)$$

We further specify the helicity states of the spinors and polarisation vectors in the tensor structures $\{T_j\}_{j=1}^8$,

$$T_1^{h_1 h_2 h_3 h_4} = \bar{u}(p_4, h_4)\slashed{p}_1 v(p_2, h_2)\, p_2 \cdot \varepsilon(p_1, q_1, h_1)\, p_2 \cdot \varepsilon(p_3, q_3, h_3)\,,$$

$$T_2^{h_1 h_2 h_3 h_4} = \bar{u}(p_4, h_4)\slashed{p}_1 v(p_2, h_2)\, p_2 \cdot \varepsilon(p_1, q_1, h_1)\, p_4 \cdot \varepsilon(p_3, q_3, h_3)\,,$$

$$T_3^{h_1 h_2 h_3 h_4} = \bar{u}(p_4, h_4)\slashed{p}_1 v(p_2, h_2)\, p_4 \cdot \varepsilon(p_1, q_1, h_1)\, p_2 \cdot \varepsilon(p_3, q_3, h_3)\,,$$

$$T_4^{h_1 h_2 h_3 h_4} = \bar{u}(p_4, h_4)\slashed{p}_1 v(p_2, h_2)\, p_4 \cdot \varepsilon(p_1, q_1, h_1)\, p_4 \cdot \varepsilon(p_3, q_3, h_3)\,, \qquad (3.23)$$

$$T_5^{h_1 h_2 h_3 h_4} = \bar{u}(p_4, h_4)\slashed{p}_3 v(p_2, h_2)\, p_2 \cdot \varepsilon(p_1, q_1, h_1)\, p_2 \cdot \varepsilon(p_3, q_3, h_3)\,,$$

$$T_6^{h_1 h_2 h_3 h_4} = \bar{u}(p_4, h_4)\slashed{p}_3 v(p_2, h_2)\, p_2 \cdot \varepsilon(p_1, q_1, h_1)\, p_4 \cdot \varepsilon(p_3, q_3, h_3)\,,$$

$$T_7^{h_1 h_2 h_3 h_4} = \bar{u}(p_4, h_4)\slashed{p}_3 v(p_2, h_2)\, p_4 \cdot \varepsilon(p_1, q_1, h_1)\, p_2 \cdot \varepsilon(p_3, q_3, h_3)\,,$$

$$T_8^{h_1 h_2 h_3 h_4} = \bar{u}(p_4, h_4)\slashed{p}_3 v(p_2, h_2)\, p_4 \cdot \varepsilon(p_1, q_1, h_1)\, p_4 \cdot \varepsilon(p_3, q_3, h_3)\,,$$

from which we obtain the contracted helicity amplitudes,

$$\tilde{A}_{5,i}^{(L),h_1 h_2 h_3 h_4} = \sum_{j,k=1}^{8} T_j^{h_1 h_2 h_3 h_4} \left(\Theta^{-1}\right)_{jk} \tilde{\mathcal{A}}_{5,k\,i}^{(L)}\,, \qquad (3.24)$$

with

$$\tilde{\mathcal{A}}_{5,k\,i}^{(L)} = \sum_{\text{pol}} T_k^\dagger \tilde{A}_{5,i}^{(L)} \,. \tag{3.25}$$

We carry out the same decomposition for the five-particle finite remainder $F_{5,d}^{(L)\mu}$, arriving at the following formula for the contracted helicity finite remainders,

$$\tilde{F}_{5,i}^{(L),h_1 h_2 h_3 h_4} = \sum_{j,k=1}^{8} T_j^{h_1 h_2 h_3 h_4} \left(\Theta^{-1}\right)_{jk} \tilde{\mathcal{F}}_{5,k\,i}^{(L)} \,, \tag{3.26}$$

where

$$\tilde{\mathcal{F}}_{5,k\,i}^{(L)} = \sum_{\text{pol}} T_k^\dagger \, p_{i\,\mu} \, F_{5,d}^{(L)\mu} \,. \tag{3.27}$$

As discussed in Section 2, the independent helicity configurations which we need to compute are

$$\left\{ \tilde{F}_{5,i}^{(L),+++-} , \tilde{F}_{5,i}^{(L),-++-} , \tilde{F}_{5,i}^{(L),+-++} , \tilde{F}_{5,i}^{(L),--++} \right\} \,. \tag{3.28}$$

We note that it is possible to compute directly the contracted finite remainders $\tilde{F}_{5,i}^{(L)}$ without specifying the helicity states. In our setup, however, such a computation would lead to more complicated analytic expressions compared to the results obtained for the contracted helicity amplitudes.

3.3 Structure of the four-particle W-production amplitudes

The four-particle W-production amplitude $A_4^{(L)\mu}$ has been computed in the context of $W+1j$ production at the LHC ($q\bar{q} \to Wg$) [7], which is a crossing of the $e^+e^- \to q\bar{q}g$ amplitude [67]. In our case it is convenient to express $A_4^{(L)\mu}$ in terms of the same special function basis as $A_{5,d}^{(L)\mu}$. This guarantees a uniform combination of the different contributions to the full amplitude. We therefore re-derive the $A_4^{(L)\mu}$ amplitude using our computational framework. We decompose the $A_4^{(L)\mu}$ amplitude using the following tensor structures [67],

$$A_4^{(L)\mu}(p_2, p_3, p_4) = \sum_{i=1}^{7} b_i^{(L)} Y_i^\mu \,, \tag{3.29}$$

where

$$
\begin{aligned}
Y_1^\mu =\ & \bar{u}(p_4)\slashed{p}_3 v(p_2)\,\varepsilon_3 \cdot p_4\, p_4^\mu - p_3 \cdot p_4\, \bar{u}(p_4)\slashed{\varepsilon}_3 v(p_2)\, p_4^\mu \\
& - (p_2 \cdot p_4 + p_3 \cdot p_4)\left[\bar{u}(p_4)\slashed{p}_3 v(p_2)\,\varepsilon_3^\mu - \bar{u}(p_4)\slashed{\varepsilon}_3 v(p_2)\, p_3^\mu\right]\,, \\
Y_2^\mu =\ & \bar{u}(p_4)\slashed{p}_3 v(p_2)\,\varepsilon_3 \cdot p_4\, p_3^\mu - p_3 \cdot p_4\, \bar{u}(p_4)\slashed{\varepsilon}_3 v(p_2)\, p_3^\mu \\
& - (p_2 \cdot p_3 + p_3 \cdot p_4)\left[\bar{u}(p_4)\slashed{p}_3 v(p_2)\,\varepsilon_3^\mu - \bar{u}(p_4)\slashed{\varepsilon}_3 v(p_2)\, p_3^\mu\right]\,, \\
Y_3^\mu =\ & \bar{u}(p_4)\slashed{p}_3 v(p_2)\,\varepsilon_3 \cdot p_4\, p_2^\mu - p_3 \cdot p_4\, \bar{u}(p_4)\slashed{\varepsilon}_3 v(p_2)\, p_2^\mu \\
& - (p_2 \cdot p_3 + p_2 \cdot p_4)\left[\bar{u}(p_4)\slashed{p}_3 v(p_2)\,\varepsilon_3^\mu - \bar{u}(p_4)\slashed{\varepsilon}_3 v(p_2)\, p_3^\mu\right]\,, \qquad (3.30) \\
Y_4^\mu =\ & \bar{u}(p_4)\slashed{p}_3 v(p_2)\,\varepsilon_3 \cdot p_2\, p_4^\mu - p_2 \cdot p_3\, \bar{u}(p_4)\slashed{\varepsilon}_3 v(p_2)\, p_4^\mu\,, \\
Y_5^\mu =\ & \bar{u}(p_4)\slashed{p}_3 v(p_2)\,\varepsilon_3 \cdot p_2\, p_3^\mu - p_2 \cdot p_3\, \bar{u}(p_4)\slashed{\varepsilon}_3 v(p_2)\, p_3^\mu\,, \\
Y_6^\mu =\ & \bar{u}(p_4)\slashed{p}_3 v(p_2)\,\varepsilon_3 \cdot p_2\, p_2^\mu - p_2 \cdot p_3\, \bar{u}(p_4)\slashed{\varepsilon}_3 v(p_2)\, p_2^\mu\,, \\
Y_7^\mu =\ & p_3 \cdot p_4\, \bar{u}(p_4)\gamma^\mu v(p_2)\,\varepsilon_3 \cdot p_2 - p_2 \cdot p_3\, \bar{u}(p_4)\gamma^\mu v(p_2)\,\varepsilon_3 \cdot p_4 \\
& - (p_2 \cdot p_3)\left[\bar{u}(p_4)\slashed{p}_3 v(p_2)\,\varepsilon_3^\mu - \bar{u}(p_4)\slashed{\varepsilon}_3 v(p_2)\, p_3^\mu\right]\,.
\end{aligned}
$$

The coefficients $b_i^{(L)}$ can be determined through

$$
b_i^{(L)} = \sum_j \left(\Omega^{-1}\right)_{ij} \tilde{A}_{4,j}^{(L)}\,, \qquad (3.31)
$$

where

$$
\Omega_{ij} = \sum_{\text{pol}} Y_i^{\mu\dagger} Y_{j\mu}\,, \qquad (3.32)
$$

$$
\tilde{A}_{4,i}^{(L)} = \sum_{\text{pol}} Y_i^{\mu\dagger} A_{4\,\mu}^{(L)}\,. \qquad (3.33)
$$

The gluon polarisation-vector sum follows from Eq. (3.22). We note that the tensor structures in Eq. (3.30) are different from the ones employed in Ref. [67]. Here, we start from 12 tensor structures that are linearly independent in 4 dimensions [62, 63] and reduce them to 7 by imposing Ward identities. Since $A_4^{(L)\mu}$ is a four-point amplitude, it does not depend on tr_5. For the sake of uniformity, we express it in terms of the five-point Mandelstam invariants $\vec{s}_5$ (3.11). In contrast to the computation of $A_{5,d}^{(L)\mu}$, here we derive the contracted amplitudes $\tilde{A}_{4,i}^{(L)}$ directly without specifying the helicity states, since the four-point computation is relatively simple. The helicity states for the tensor structures Y_μ^i are specified when the decay currents are attached, following Eq. (3.2).

Once again we perform the same decomposition on the corresponding four-particle finite remainder $F_4^{(L)\mu}$. The resulting formula for the contracted finite remainders is

$$
\tilde{F}_{4,i}^{(L)} = \sum_{\text{pol}} Y_i^{\mu\dagger} F_{4\,\mu}^{(L)}\,. \qquad (3.34)
$$

3.4 Amplitude reduction and analytic reconstruction

In this section we present the analytic computation of the contracted five- and four-particle finite remainders, $\tilde{F}_{5,i}^{(L),h_1h_2h_3h_4}$ (3.26) and $\tilde{F}_{4,i}^{(L)}$ (3.34) respectively, at one and two loops. We adopt the framework used in Refs. [41–43, 68], based on Feynman diagrams and functional reconstruction from numerical sampling over finite field. For the latter we employ the FINITEFLOW framework [54].

In order to use the finite field technique, we need to have a rational parameterisation of the kinematics. As discussed in Section 3.1, the five-particle phase space is described by the six scalar invariants $\vec{s}_5$ (3.11) together with the pseudo-scalar invariant tr_5 (3.9). It follows from Eq. (3.10) that tr_5 is given by the square root of Δ_5, up to the overall sign which encodes the parity information. This square root may be dealt with in two ways: either parameterise the kinematics to explicitly rationalise $\sqrt{\Delta_5}$, or parameterise the finite remainders $\tilde{F}_{5,i}^{(L),h_1h_2h_3h_4}$ such that the dependence on tr_5 is analytic. We choose the latter option in this case. The pseudo-scalar invariant tr_5 can enter the computation in three distinct ways. First, it can originate from the γ_5 in the axial coupling of the W boson. As we discussed in Section 2, we set up the computation so that only the vector coupling of W is used. Second, tr_5 is in general needed to capture the parity-odd part of the spinor-helicity expressions. However, the pseudo-scalar invariant enters the contracted helicity finite remainder in Eq. (3.26) only through the spanning basis elements $T_j^{h_1h_2h_3h_4}$, which are known analytically and do not need to be reconstructed over finite fields. Finally, tr_5 is present in the definition of the canonical master integrals, which also introduces three other square roots, $\sqrt{\Delta_3^{(i)}}$ with $i = 1, 2, 3$, relevant for the analytic structure of the Feynman integrals [48, 51]. Since the square roots appear only as overall normalisation factors, we can re-absorb them in the definition of the canonical master integrals, and thus reduce the finite remainders to master integrals which are all manifestly scalar. With this setup the only parts of the contracted finite remainders which need to be reconstructed are rational functions of the scalar invariants $\vec{s}_5$ only, and can thus be sampled numerically over finite fields.

The starting point of our computation is the expression of the W-production five- and four-particle amplitudes, $A_{5,d}^{(L)\mu}$ and $A_4^{(L)\mu}$, in terms of Feynman diagrams, which we generate using QGRAF [69]. For those interested in counting Feynman diagrams, there are 20 diagrams for $A_{5,d}^{(1),1\mu}$, 231 diagrams for $A_{5,d}^{(2),1\mu}$, 32 diagrams for $A_{5,d}^{(2),n_f\mu}$, 7 diagrams for $A_4^{(1),1\mu}$, 74 diagrams for $A_4^{(2),1\mu}$, and 13 diagrams for $A_4^{(2),n_f\mu}$. Clearly this signifies nothing more than that the number of diagrams is not a good measure of complexity. We want to obtain analytic, IBP-compatible expressions for the contracted amplitudes, $\tilde{A}_{5,i}^{(L),h_1h_2h_3h_4}$ and $\tilde{A}_{4,i}^{(L)}$. For the four-point amplitude $A_4^{(L)\mu}$ we apply the projectors and sum over all polarisation states as in Eq. (3.33). For the five-point amplitude $A_{5,d}^{(L)\mu}$ we contract by the external momenta and apply the projectors, as in Eqs. (3.17) and (3.25), respectively. We then rewrite the resulting expressions in terms of scalar Feynman integrals belonging to the master topologies defined in Refs. [42, 43]. We carry out all these operations analytically using MATHEMATICA and FORM [70, 71] scripts. As a result, we obtain analytic expressions

for $\tilde{\mathcal{A}}_{5,i\,k}^{(L)}$ (3.25) and $\tilde{A}_{4,i}^{(L)}$ (3.33) as linear combinations of scalar Feynman integrals with rational coefficients functions of $\vec{s}_5$. In order to obtain the contracted helicity-amplitudes $\tilde{A}_{5,i}^{(L),h_1h_2h_3h_4}$ from the $\tilde{\mathcal{A}}_{5,i\,k}^{(L)}$'s we further need to multiply by the spanning basis elements $T_j^{h_1h_2h_3h_4}$ and by the inverse of Θ, as shown in Eq. (3.24). We do these operations (including the inversion of Θ) numerically within the finite field framework.

We reduce the scalar integrals to the canonical master integrals identified in Ref. [48], which we modified so as to re-absorb the square roots. We generate the IBP relations [56] using LiteRed [72] in Mathematica, and solve them numerically over finite fields using the Laporta algorithm [57] through FiniteFlow's linear solver. We then perform a Laurent expansion of the rational coefficients around $\epsilon = 0$, and map the canonical master integrals onto square roots and the special function basis of Ref. [42] up to the required order in ϵ. We label the special function basis by $\{f_k\}$. We truncate the ϵ expansion at order ϵ^2 at one loop and at order ϵ^0 at two loops. Finally, we subtract the UV/IR poles as in Eq. (2.15) and define the contracted finite remainders, which we represent as

$$
\begin{aligned}
\tilde{F}_{5,i}^{(L),h_1h_2h_3h_4} &= \Phi_5^{h_1h_2h_3h_4} \sum_j \left[q_{i,j}^{h_1h_2h_3h_4}(\vec{s}_5) + \mathrm{tr}_5\, r_{i,j}^{h_1h_2h_3h_4}(\vec{s}_5) \right] \mathrm{mon}_j \left(\mathrm{tr}_5, \sqrt{\Delta_3^{(l)}}, \{f_k\} \right) , \\
\tilde{F}_{4,i}^{(L)} &= \sum_j t_{i,j}(\vec{s}_5)\, \mathrm{mon}_j \left(\mathrm{tr}_5, \sqrt{\Delta_3^{(l)}}, \{f_k\} \right) ,
\end{aligned}
\tag{3.35}
$$

where $\mathrm{mon}_j(x,y,\dots)$ denotes monomials in $x, y, \dots$, while $q_{i,j}^{h_1h_2h_3h_4}$, $r_{i,j}^{h_1h_2h_3h_4}$ and $t_{i,j}$ are rational functions of $\vec{s}_5$. Note that we pull out from the five-particle finite remainders an arbitrary phase factor $\Phi_5^{h_1h_2h_3h_4}$ carrying all the helicity weights, so that the coefficients $q_{i,j}^{h_1h_2h_3h_4}$ and $r_{i,j}^{h_1h_2h_3h_4}$ are scalar and hence functions of $\vec{s}_5$ only. We recall that the helicity configuration is assigned to the four-particle finite remainders when attaching the decay current, as discussed in Section 3.3. The cancellation of the poles at this stage provides a robust check of the result prior to the rational reconstruction. Furthermore, it typically leads to simplifications which make the finite remainders easier to reconstruct than the bare amplitudes. This chain of operations is implemented in the FiniteFlow framework, and ultimately amounts to an algorithm which samples numerically over finite fields the rational coefficients in the contracted finite remainders.

Finally, we need to reconstruct the rational coefficients of the contracted finite remainders from their numerical values. Following Refs. [28, 41–43], we perform a number of optimisations to reduce the number of required sample points. We follow the strategy outlined in Ref. [41]. First of all, we set $s_{12} = 1$. We recover the analytic dependence on s_{12} a posteriori through dimensional analysis. Second, we fit the $\mathbb{Q}$-linear relations among the rational coefficients, and solve them so as to express the most complicated coefficients in terms of the simplest ones. Third, we reconstruct the coefficients on a random univariate phase-space slice modulo a large prime number, and match them with ansätze made of the

following factors (with $s_{12} = 1$):

$$\Big\{ s_{12} \,, s_{23} \,, s_{34} \,, s_{23} + s_{34} \,, s_{23} - s_{234} \,, s_{234} - s_{34} \,, s_{123} - s_{56} \,, s_{234} - s_{56} \,, s_{12} - s_{123} + s_{23} \,,$$

$$s_{12} + s_{234} - s_{34} \,, s_{23} - s_{234} + s_{34} \,, s_{12} + s_{234} - s_{56} \,, s_{12} - s_{123} - s_{34} \,, s_{123}s_{234} - s_{23}s_{56} \,,$$

$$s_{12} - s_{123} + s_{23} - s_{34} \,, s_{123} - s_{23} + s_{234} - s_{56} \,, s_{12} + s_{234} - s_{34} - s_{56} \,,$$

$$s_{12}s_{234} - s_{123}s_{234} + s_{23}s_{234} - s_{234}s_{34} + s_{34}s_{56} \,,$$

$$s_{12}s_{234} - s_{123}s_{234} - s_{234}s_{34} + s_{23}s_{56} + s_{34}s_{56} \,, s_{12}s_{234} + s_{234}^2 - s_{234}s_{34} - s_{234}s_{56} + s_{34}s_{56} \,,$$

$$s_{12}s_{123} + s_{123}s_{234} - s_{123}s_{34} - s_{12}s_{56} - s_{23}s_{56} \,, s_{12}s_{123} - s_{123}^2 - s_{123}s_{34} - s_{12}s_{56} + s_{123}s_{56} \,,$$

$$s_{12}^2 - s_{12}s_{123} + s_{12}s_{234} - s_{123}s_{234} - 2s_{12}s_{34} + s_{123}s_{34} - s_{234}s_{34} + s_{34}^2 + s_{23}s_{56} \,,$$

$$s_{12}s_{23} - s_{12}s_{234} + s_{23}s_{234} - s_{234}^2 - s_{23}s_{34} + s_{234}s_{34} - s_{23}s_{56} + s_{234}s_{56} - s_{34}s_{56} \,,$$

$$\lambda \left(s_{12}, s_{34}, s_{56} \right) , \lambda \left(s_{23}, s_{14}, s_{56} \right) , \mathrm{tr}_5^2 \Big\} \,,$$

$$(3.36)$$

where λ is the Källen function,

$$\lambda(a, b, c) = a^2 + b^2 + c^2 - 2ab - 2bc - 2ca \,. \qquad (3.37)$$

The factors in the list (3.36) are a subset of the letters of the (planar) one-mass pentagon alphabet [48], namely of the arguments of the logarithmic integration kernels appearing in the differential equations satisfied by the master integrals. The letters govern the singularity structure of the master integrals and hence of the special function basis $\{f_k\}$. It is therefore natural to expect that the denominators of the rational coefficients multiplying the special functions should factorise in terms of letters, and indeed the previous experience has shown that this is the case [28, 41–43]. It follows that we can determine entirely the denominators of the rational coefficients by matching them against ansätze made of the factors in Eq. (3.36) on a univariate slice. Part of the numerators may in general be caught by this approach as well. In Table 1 we show the impact of this strategy on the highest polynomial degrees of the rational coefficients which need to be reconstructed for the five-particle contracted finite remainders. Note that we process all helicity configurations of the five-particle finite remainders simultaneously, but for the n_f^0 ones we separate the contractions by the external momenta into two subsets, $\{p_1, p_2\}$ and $\{p_3, p_4\}$, to reduce the memory usage. After this optimisation is done, the rational coefficients are reconstructed using the multivariate functional reconstruction algorithms implemented in FINITEFLOW [54].

3.5 Simplification of the rational coefficients

The resulting analytic expressions of the rational coefficients of the finite remainders are rather bulky. The standard approach to simplify them relies on partial fraction decomposition, either multivariate [30, 73–77] or univariate with respect to a suitable variable [41–44]. For the rational coefficients of the four-point finite remainders, $t_{i,j}\left(\vec{s}_5 \right)$ in Eq. (3.35), we achieve a satisfactory simplification by performing a multivariate partial fraction decomposition with the MATHEMATICA package MULTIVARIATEAPART [76], enhanced by SINGULAR [78] for the computation of the Gröbner bases.

	$s_{12} = 1$	linear relations	factor matching
$\tilde{F}_{5,i}^{(2),1\,h_1 h_2 h_3 h_4}$ with $i = 1, 2$	44/44	41/40	41/0
$\tilde{F}_{5,i}^{(2),1\,h_1 h_2 h_3 h_4}$ with $i = 3, 4$	48/47	42/42	42/0
$\tilde{F}_{5,i}^{(2),n_f\,h_1 h_2 h_3 h_4}$ with $i = 1, 2, 3, 4$	39/38	26/24	26/0

Table 1: Maximal total polynomial degrees of the rational coefficients of the contracted two-loop five-particle finite remainders at each stage of the optimisation procedure for the finite-field reconstruction, in the form numerator/denominator. The coefficients are functions of the five scalar invariants $\{s_{23}, s_{34}, s_{123}, s_{234}, s_{56}\}$ ($s_{12} = 1$). The independent helicity configurations (3.28) are processed simultaneously, while the contractions by the external momenta for $\tilde{F}_{5,i}^{(2),1\,h_1 h_2 h_3 h_4}$ are separated into two subsets to reduce the memory usage.

The rational coefficients of the five-particle finite remainders are instead substantially more involved. In order to simplify them, we look for a parameterisation of the five-particle kinematics leading to more compact expressions than the scalar invariants $\vec{s}_5$ (3.11). We investigate how the complexity of the expressions varies when using momentum-twistor parameterisations [64]. The pseudo-scalar invariant tr_5 is given by a rational function in terms of momentum-twistor variables, and we can thus add up the two terms of the coefficients of the special function monomials,

$$\left(q_{i,j}^{h_1 h_2 h_3 h_4}\left(\vec{s}_5 \right) + \mathrm{tr}_5 \ r_{i,j}^{h_1 h_2 h_3 h_4}\left(\vec{s}_5 \right) \right)\bigg|_{\vec{s}_5 = \vec{s}_5(\vec{z})} = u_{i,j}^{h_1 h_2 h_3 h_4}\left(\vec{z} \right) , \qquad (3.38)$$

where by $\vec{z} = \{z_i\}_{i=1,\dots,6}$ we denote generally the independent momentum-twistor variables. In particular, we consider the parameterisation proposed in Ref. [43],

$$z_1 = s_{12}, \qquad\qquad z_2 = -\frac{\mathrm{tr}_+(1234)}{s_{12}s_{34}},$$

$$z_3 = \frac{\mathrm{tr}_+(1341(5+6)2)}{s_{13}\,\mathrm{tr}_+(14(5+6)2)}, \qquad z_4 = \frac{s_{23}}{s_{12}}, \qquad\qquad (3.39)$$

$$z_5 = -\frac{\mathrm{tr}_-(1(2+3)(1+5+6)(5+6)23)}{s_{23}\,\mathrm{tr}_-(1(5+6)23)}, \qquad z_6 = \frac{s_{456}}{s_{12}}.$$

In previous applications, such a parameterisation has been used globally, i.e. in all amplitudes/finite remainders irrespective of their helicity configuration. We find that this approach does not perform well in this case, and does not lead to a major simplification in comparison with the expressions in terms of scalar invariants $\vec{s}_5$ and tr_5. The rational parameterisation has the effect of breaking some symmetries in the kinematic quantities, which results in some configurations being simpler than others. There is no reason for the parameterisation to be a global choice, and in this case we exploit this fact and consider different parameterisations for each helicity configuration.

In practice, we consider all parameterisations which are obtained by permuting the massless momenta on the right-hand side of Eqs. (3.39). For each helicity configuration

we determine which permutations of the parameterisation lead to the most compact expression of the finite remainder at one loop. We then use them at two loops, and select the one which results in the simplest expression. We perform the change of variables over finite fields within the FINITEFLOW framework, and measure the "simplicity" of the rational coefficients in terms of their numerator/denominator polynomial degrees, which can be determined without reconstructing the expression of the coefficients in terms of the new variables. Once the "best" parameterisation $\vec{s}_5 = \vec{s}_5(\vec{z})$ is chosen for each helicity configuration, we reconstruct the analytic expression of the coefficients in terms of the new variables $\vec{z}$. For this purpose we make use of the finite field algorithm for univariate partial fraction decomposition presented in Refs. [41, 42]. We choose the variable to partial fraction with respect to so as to minimise the polynomial degrees of the separate terms of the decomposition. Breaking down the coefficients into univariate partial fractions simplifies the subsequent multivariate partial fraction decomposition, which we perform using MULTIVARIATEAPART [76] enhanced with SINGULAR [78]. We apply it to each term of the univariate partial fraction decomposition separately, which is convenient as each term is by itself much simpler than the full coefficient. This is possible because MULTIVARIATEA-PART's algorithm commutes with summation by design. The spurious poles introduced by the univariate partial fraction decomposition therefore cancel out after the multivariate partial fraction decomposition. In summary, our algorithm for the simplification of the rational coefficients of the five-particle finite remainders is the following.

1. Try all permutations of a given momentum-twistor parameterisation on the one-loop expressions and select the ones which lead to the lowest polynomial degrees.

2. Apply the parameterisations selected at step 1 on the two-loop rational coefficients and choose the one which leads to the lowest polynomial degree.

3. Decompose the two-loop rational coefficients in terms of the new variables into univariate partial fractions with respect to the variable which leads to the lowest polynomial degrees in the separate terms.

4. Decompose into multivariate partial fractions the separate terms of the univariate partial fractions using the algorithm of Ref. [76], and sum them up cancelling the spurious poles.

In hindsight, the first three steps could have been implemented within the original FINITE-FLOW setup. We did not attempt this approach because we did not need any further optimisation to reconstruct the rational coefficients of the W-production five-particle finite remainders. However, we believe that this strategy may also help to improve the rational reconstruction.

We apply this procedure separately on each of the helicity configurations, leading to different parameterisations for each of them. The resulting expressions for the coefficients are remarkably more compact than the original ones in terms of the scalar invariants $\vec{s}_5$. For the most complicated finite remainder we achieved a compression in the file size of more than two orders of magnitude. The evaluation time of the rational coefficients is similarly improved.

3.6 Numerical evaluation and permutations of the amplitudes

In order to obtain the values of all the amplitudes in all the possible scattering channels we need to evaluate the minimal set of independent objects we reconstructed for different permutations of the external momenta (see e.g. Eq. (2.8) for an explicit example). In this subsection we discuss how we implement this operation in an efficient way at the level of the numerical evaluation.

We denote a generic permutation of the external momenta by

$$\sigma = (\sigma_1 \sigma_2 \sigma_3 \sigma_4 \sigma_5 \sigma_6) \,, \tag{3.40}$$

where the σ_i's take distinct values in $\{1, 2, 3, 4, 5, 6\}$, such that the action of σ on an external momentum is given by

$$\sigma \circ p_i = p_{\sigma_i} \,. \tag{3.41}$$

Not all S_6 permutations of $\{1, 2, 3, 4, 5, 6\}$ are needed for this application. The required permutations belong to the subset $S_4 \times Z_2$, i.e. they are obtained by composing an S_4 permutation of $\{p_1, p_2, p_3, p_4\}$ and a Z_2 exchange of $\{p_5, p_6\}$. In particular, p_5 and p_6 need to be exchanged in order to obtain the $W^-\gamma j$ amplitudes according to Eq. (2.18). Only the S_4 permutations are relevant for the W-production amplitudes (and hence for the special functions), since p_5 and p_6 enter them only in the sum $p_5 + p_6$ (see e.g. Eqs. (3.1) and (3.2)). The Z_2 exchange is relevant only for the leptonic currents ($L_{A,\mu}$ and $L_{B,\mu}^{e/W}$), which are rational functions.

Given a generic amplitude/finite remainder A, function of the external momenta $\{p_i\}$, we define its permutation σ as

$$(\sigma \circ A)(\{p_i\}) = A(\{\sigma \circ p_i\}) \,. \tag{3.42}$$

In other words, we can obtain the value of the permuted amplitude by evaluating the amplitude in the original orientation of the external momenta at a permuted phase space point. While this operation is trivial for the rational functions, it is in general very subtle for the special functions. The reason is that a permutation in general maps the phase-space point to a different scattering region. This would require a complicated analytic continuation, since the special functions have a very intricate branch cut structure.

One way to overcome this problem is to evaluate the special functions numerically using the generalised series expansion method [79], implemented in the public MATHEMATICA package DIFFEXP [80], as done in Refs. [42, 43]. Within this method the analytic continuation can be carried out systematically. This approach however requires that, for each phase-space point where we want to evaluate the permuted amplitudes, we evaluate the special functions at as many points as the number of needed permutations.

For phase-space points in the physical scattering region we can adopt a much more efficient evaluation strategy: we use the C++ package PENTAGONFUNCTIONS++ [51], which allows us to evaluate in the physical scattering region a larger basis of special functions, named one-mass pentagon functions. We denote them by $\{g_i\}$. For this purpose we translate

the special function basis $\{f_i\}$ of Ref. [42] to the one-mass pentagon function basis $\{g_i\}$ implemented in PENTAGONFUNCTIONS++. The translation takes the form

$$f_i = \sum_j w_{ij} \operatorname{mon}_j\left(\{g_k\}\right) , \tag{3.43}$$

where $w_{ij} \in \mathbb{Q}$, and the sum runs over all the required monomials of the one-mass pentagon functions $\{g_k\}$. We obtain the transformation rules (3.43) by matching the expressions of the master integrals in terms of special special functions given in Ref. [42] with that of Ref. [51]. The advantage of the one-mass pentagon functions with respect to the function basis $\{f_i\}$ or Ref. [42] is that their evaluation through the package PENTAGONFUNCTIONS++ is extremely efficient, and their design allows us to generate the values of all S_4 permutations of the functions from those at the un-permuted phase-space point. The one-mass pentagon function basis $\{g_i\}$ is in fact closed under S_4 permutations. This means that, for any $\sigma \in S_4$, we can express the permuted one-mass pentagon functions evaluated at a given phase-space point as a combination of un-permuted pentagon functions evaluated at the same point,

$$\left(\sigma \circ g_i\right)\left(\vec{s}_5, \operatorname{tr}_5\right) = \sum_j \Sigma_{ij}^{(\sigma)} \operatorname{mon}_j\left[\{g_k\left(\vec{s}_5, \operatorname{tr}_5\right)\}\right] , \tag{3.44}$$

where $\Sigma_{ij}^{(\sigma)} \in \mathbb{Q}$, and we spelled out the dependence on the kinematics for the sake of clarity. These transformation rules are provided in Ref. [51].[1] This strategy is advantageous because it minimises the number of evaluations of the special functions, which is the most time-consuming step in the numerical evaluation of the colour and helicity summed squared amplitudes.

It is worth highlighting the special behaviour of the pseudo-scalar invariant tr_5 in this chain of operations. In the physical scattering regions the reality of the momenta implies that $\operatorname{tr}_5^2 < 0$. In other words, tr_5 is purely imaginary. The library PENTAGONFUNC-TIONS++ always assumes that $\operatorname{Im}\left[\operatorname{tr}_5\right] > 0$. The sign of tr_5 however may change upon the action of an odd-signature permutation,

$$\sigma \circ \operatorname{tr}_5 = \operatorname{sign}(\sigma)\operatorname{tr}_5 , \tag{3.45}$$

or space-time parity. The values of the one-mass pentagon functions for a negative imaginary part of tr_5 can be obtained by flipping the sign of a subset of functions specified in Ref. [51]. In our setup however we do not need to. As discussed in Section 3.4, we reduce the amplitudes to manifestly scalar master integrals, and group together the special functions and the square roots arising from the definition of the canonical master integrals. As a result, the monomials of special functions and square roots in the finite remainders (3.35)

---

[1]Note that Ref. [51] has a different labelling of the external momenta. Moreover, the package PEN-TAGONFUNCTIONS++ works in a specific physical scattering region (the s_{45} channel using the notation of Ref. [51]). A relabelling and a further permutation of the momenta are required to use PENTAGONFUNC-TIONS++ in the scattering region relevant for our application. We implemented these operations in the MATHEMATICA evaluation script provided in the ancillary files, and refer to the original work [51] for a discussion of how to use PENTAGONFUNCTIONS++ in a physical region different from the default one.

are scalar as well. Any sign change in the pentagon functions due to permutations or space-time parity is therefore compensated by that of the accompanying factor of tr_5, and we can thus evaluate both with a value of tr_5 such that $\text{Im}[\text{tr}_5] > 0$ — as by default in PentagonFunctions++ — regardless of the permutations or space-time parity. We must only keep track of the sign of tr_5 in the rational coefficients (see Eqs. (3.35)), which enters our final expressions for the five-particle finite remainders through the values of the momentum twistors, and is determined by the values of the external momenta through its definition (3.9). The same holds for the other square roots in the problem, $\sqrt{\Delta_3^{(i)}}$, which appear only in the special function monomials. The polynomials $\Delta_3^{(i)}$ are positive in the physical scattering regions. We adopt the convention of Ref. [51] that their square roots are positive, $\sqrt{\Delta_3^{(i)}} > 0$, as done in PentagonFunctions++.

In conclusion, we reconstruct the analytic expressions for the minimal set of independent finite remainders, and generate the values of the remaining ones by permuting the former at the numerical evaluation stage. We do this by evaluating the rational coefficients at permuted points, whereas we obtain the values of all permutations of the special functions from the values of the functions at the original phase-space point only. This allows us to minimise the amount of analytic data, whose size may otherwise become problematic, and at the same time evaluate the results efficiently.

4 Validation

In this section we discuss a number of validations performed on the analytic results derived in this work. First, let us remind the readers that the quantities that we reconstructed analytically are the L-loop finite remainders, where the UV and IR poles contained in the L-loop bare amplitudes are cancelled by the pole terms according to Eq. (2.15). These pole cancellations already provide a strong consistency check of our calculation. In the following subsections we present further checks.

4.1 Comparison against full six-point computation

In order to verify the analytic expressions obtained by detaching the leptonic decay current as described in Section 3, we cross-check them against the helicity amplitudes obtained by computing the six-point process directly using a framework that has been applied to the computation of several two-loop amplitudes [41, 43, 68, 81]. We perform the full six-point computation numerically using the momentum twistor parameterisation (3.13) by assigning rational values to the variables $x_1, \ldots, x_8$ in the rational coefficients and treating the special functions symbolically. We derive numerical results for all the sub-amplitudes — $A_{6,u}^{(L)}$, $A_{6,d}^{(L)}$, $A_{6,W}^{(L)}$ and $A_{6,e}^{(L)}$ — in all four contributing helicity configurations. We find full numerical agreement between the two approaches. This provides a further robust check of our analytic computation, where we derived analytic expressions only for the independent helicity configurations and obtained the remaining ones by complex conjugation and permutation of the external momenta.

4.2 Gauge invariance

The gauge-invariance structure of the $W^+\gamma j$ amplitude is slightly complicated by the different sources of photon emission, as discussed in Section 2. The individual sub-amplitudes ($A_{6,i}^{(L)}$ with $i = u, d, W, e$) are not separately gauge invariant in the electroweak (EW) sector. Only linear combinations of them, defined in Eq. (2.6), are. We rewrite them here for convenience,

$$\left\{ A_{6,u}^{(L)} + \frac{1}{s_{156} - s_{56}} A_{6,W}^{(L)}, \quad A_{6,d}^{(L)} - \frac{1}{s_{156} - s_{56}} A_{6,W}^{(L)}, \quad A_{6,e}^{(L)} - \frac{1}{s_{156} - s_{56}} A_{6,W}^{(L)} \right\}. \quad (4.1)$$

We verify explicitly that these combinations satisfy the EW Ward identity by replacing the photon polarisation vector with its momentum ($\varepsilon(p_1) \to p_1$) and checking that the resulting expressions vanish.

The QCD Ward identity (performed by replacing the gluon polarisation vector with its momentum, $\varepsilon(p_3) \to p_3$), instead, is already satisfied by the individual sub-amplitudes. We checked this explicitly as well.

We further demonstrate the gauge invariance by evaluating the helicity amplitudes using two different sets of reference momenta for the photon and gluon polarisation vectors (q_1 and q_3), finding perfect agreement.

4.3 Renormalisation scale dependence

The L-loop finite remainders depend on the renormalisation scale, μ. In deriving analytic results for the process $W^+\gamma j$ we set the renormalisation scale to unity ($\mu = 1$). The dependence on the renormalisation scale of the finite remainders can be restored as follows,

$$F_6^{(L),i}\left(\mu^2\right) = F_6^{(L),i}\left(\mu^2 = 1\right) + \delta F_6^{(L),i}\left(\mu^2\right), \quad (4.2)$$

where we omitted the dependence on the external momenta to simplify the notation. The μ-restoring terms $\delta F_6^{(L),i}$ are built out of the lower-loop finite remainders evaluated at $\mu^2 = 1$ and logarithms of μ^2. Explicitly, they are given by

$$\delta F_6^{(1),1}\left(\mu^2\right) = \frac{11}{6} A_6^{(0)} \log\left(\mu^2\right), \quad (4.3)$$

$$\delta F_6^{(1),n_f}\left(\mu^2\right) = -\frac{1}{3} A_6^{(0)} \log\left(\mu^2\right), \quad (4.4)$$

$$\delta F_6^{(2),1}\left(\mu^2\right) = \log(\mu^2)\left\{ \left(\frac{1813}{216} - \frac{11}{36}\pi^2 + 8\zeta_3\right) A_6^{(0)} + \frac{11}{2} F_6^{(1),1}(1) \right\} + \frac{121}{24} A_6^{(0)} \log^2(\mu^2), \quad (4.5)$$

$$\delta F_6^{(2),n_f}\left(\mu^2\right) = \log(\mu^2)\left\{ \left(\frac{\pi^2}{18} - \frac{77}{18}\right) A_6^{(0)} - F_6^{(1),1}(1) + \frac{11}{2} F_6^{(1),n_f}(1) \right\} - \frac{11}{6} A_6^{(0)} \log^2(\mu^2), \quad (4.6)$$

$$\delta F_6^{(2),n_f^2}\left(\mu^2\right) = \log(\mu^2)\left\{ \frac{10}{27} A_6^{(0)} - F_6^{(1),n_f}(1) \right\} + \frac{1}{6} A_6^{(0)} \log^2(\mu^2). \quad (4.7)$$

The dependence on the external momenta is understood. We can then use Eq. (4.2) to check that the finite remainders we computed have the correct scale dependence. We do

this by evaluating the finite remainders at two phase-space points that are connected by a rescaling by some positive factor a,

$$\vec{p} = (p_1, p_2, p_3, p_4, p_5, p_6)\,,$$
$$\vec{p}\,' = a\,\vec{p} = (a\,p_1, a\,p_2, a\,p_3, a\,p_4, a\,p_5, a\,p_6)\,. \tag{4.8}$$

These two evaluations allow us to confirm numerically that the finite remainders exhibit the correct scaling behaviour, in the form

$$\frac{F_6^{(L),i}\left(1, a\,\vec{p}\right) + \delta F_6^{(L),i}\left(a^2, a\,\vec{p}\right)}{A_6^{(0)}\left(a\,\vec{p}\right)} = \frac{F_6^{(L),i}\left(1, \vec{p}\right)}{A_6^{(0)}\left(\vec{p}\right)}\,, \tag{4.9}$$

where we have made the dependence on the kinematic point explicit.

4.4 Tree-level and one-loop checks

We validated the tree-level and one-loop amplitudes derived in this paper against the results available in the literature. For the tree-level amplitude we compared our helicity amplitudes against the analytic results presented in Ref. [9] and additionally, for the full colour tree-level squared matrix elements, against MADGRAPH5 [82] for both processes $W^+\gamma j$ and $W^-\gamma j$. As for the one-loop amplitudes, we compared our results against the leading colour contributions of the $W^+\gamma j$ amplitudes presented in Ref. [9]. In all cases we find perfect agreement. We would like to point out that our choice of reference vectors for the photon and the gluon is different from the one used in Ref. [9]. For this reason we compared the gauge invariant combinations of sub-amplitudes shown in Eq. (4.1). This check therefore further validates the gauge invariance of our result.

4.5 Four-point amplitude comparison

We performed a cross check of the four-point amplitudes $A_4^{(L)\mu}$ which contribute to the sub-amplitudes $A_{6,W}^{(L)}$ and $A_{6,e}^{(L)}$ against the results provided in Ref. [7] for the scattering process $q\bar{q} \to Vg$. In Ref. [7] analytic results are presented for the helicity coefficients which are linear combinations of the form factors $b_i^{(L)}$ in Eq. (3.29), evaluated at $\mu^2 = s_{234}$. In order to enable a direct comparison for the one- and two-loop leading colour finite remainders, we recomputed the $A_4^{(L)\mu}$ amplitudes in Eq. (3.29) using the tensor structures employed in Ref. [7]. Since we compute the finite remainders with $\mu^2 = 1$, we obtain the results at $\mu^2 = s_{234}$ using the formulae to restore the dependence on μ shown in Section 4.3. We obtain perfect numerical agreement for the helicity coefficients. We further check that the four-particle finite remainders $F_4^{(L)\mu}$ computed using the tensor structures of Ref. [7] match the ones we derived using the tensor structures defined in Section 3.3 after contracting them with the decay currents according to Eq. (3.4).

5 Results

We provide analytic expressions for the five- and four-point contracted amplitudes ($\tilde{A}_{5,i}^{(L)}$ and $\tilde{A}_{4,i}^{(L)}$), at one and two loops, together with the decay currents ($L_{A,\mu}$, $L_{B,\mu}^e$, $L_{B,\mu}^W$) and the

relevant projection matrices (Δ (3.16) and Ω (3.32)) in the ancillary files. The amplitudes are presented as linear combinations of independent rational coefficients that multiply a monomial basis of square roots and special functions.

We confirm the previous observations about the cancellation of the pentagon functions involving certain letters [42–44]. We observe that the functions involving the letters $\mathcal{Z} = \{W_{18}, W_{25}, W_{34}, W_{45}, W_{46}, W_{57}\}$ (in the notation of Refs. [47, 51]) are present in the contributing integrals but drop out from the amplitudes truncated at order ϵ^0,[2] and that the functions involving the letter $W_{198} = \mathrm{tr}_5$ are present in the amplitudes and drop out from the finite remainders. The latter phenomenon is by now well established in the case of fully massless scattering, where it has been linked to an underlying cluster algebra structure of the letter alphabet [83].

We include a MATHEMATICA script to demonstrate the assembly of both the $W^+\gamma j$ and $W^-\gamma j$ amplitudes, and to perform the numerical evaluation of the finite remainders at a given kinematic point. We evaluate the special functions in the physical scattering region using the package PENTAGONFUNCTIONS++ [51], as discussed in Section 3.6.

We use the following configuration of momenta,

$$-p_2 - p_4 \to p_1 + p_3 + p_5 + p_6\,, \tag{5.1}$$

to define the six scattering channels for $pp \to W^+\gamma j$ production,

$$
\begin{aligned}
\mathbf{u\bar{d}}: \quad & u(-p_2) + \bar{d}(-p_4) \to \gamma(p_1) + g(p_3) + \nu_e(p_5) + e^+(p_6)\,, \\
\mathbf{\bar{d}u}: \quad & \bar{d}(-p_2) + u(-p_4) \to \gamma(p_1) + g(p_3) + \nu_e(p_5) + e^+(p_6)\,, \\
\mathbf{ug}: \quad & u(-p_2) + g(-p_4) \to \gamma(p_1) + d(p_3) + \nu_e(p_5) + e^+(p_6)\,, \\
\mathbf{gu}: \quad & g(-p_2) + u(-p_4) \to \gamma(p_1) + d(p_3) + \nu_e(p_5) + e^+(p_6)\,, \\
\mathbf{\bar{d}g}: \quad & \bar{d}(-p_2) + g(-p_4) \to \gamma(p_1) + \bar{u}(p_3) + \nu_e(p_5) + e^+(p_6)\,, \\
\mathbf{g\bar{d}}: \quad & g(-p_2) + \bar{d}(-p_4) \to \gamma(p_1) + \bar{u}(p_3) + \nu_e(p_5) + e^+(p_6)\,,
\end{aligned} \tag{5.2}
$$

and similarly for $pp \to W^-\gamma j$ production,

$$
\begin{aligned}
\mathbf{d\bar{u}}: \quad & d(-p_2) + \bar{u}(-p_4) \to \gamma(p_1) + g(p_3) + e^-(p_5) + \bar{\nu}_e(p_6)\,, \\
\mathbf{\bar{u}d}: \quad & \bar{u}(-p_2) + d(-p_4) \to \gamma(p_1) + g(p_3) + e^-(p_5) + \bar{\nu}_e(p_6)\,, \\
\mathbf{dg}: \quad & d(-p_2) + g(-p_4) \to \gamma(p_1) + u(p_3) + e^-(p_5) + \bar{\nu}_e(p_6)\,, \\
\mathbf{gd}: \quad & g(-p_2) + d(-p_4) \to \gamma(p_1) + u(p_3) + e^-(p_5) + \bar{\nu}_e(p_6)\,, \\
\mathbf{\bar{u}g}: \quad & \bar{u}(-p_2) + g(-p_4) \to \gamma(p_1) + \bar{d}(p_3) + e^-(p_5) + \bar{\nu}_e(p_6)\,, \\
\mathbf{g\bar{u}}: \quad & g(-p_2) + \bar{u}(-p_4) \to \gamma(p_1) + \bar{d}(p_3) + e^-(p_5) + \bar{\nu}_e(p_6)\,.
\end{aligned} \tag{5.3}
$$

The interference between the L-loop finite remainders and the tree-level amplitudes summed over colour and helicity in the leading colour approximation is given by

$$\sum_{\text{colour}} \sum_{\text{helicity}} \mathcal{A}_6^{(0)*} \mathcal{F}_6^{(L)} =: 2e^2 g_W^4 g_s^2 n^L N_c^2 \, \mathcal{H}^{(L)}\,, \tag{5.4}$$

---

[2]This holds for the set of independent amplitudes we reconstructed explicitly, which receive contributions only from the cyclic permutations of the master integrals. Since the set of letters $\mathcal{Z}$ is not closed under all S_4 permutations, these letters are present in some of the permuted amplitudes which contribute to the helicity and colour summed squared finite remainders.

where the *reduced squared finite remainder* $\mathcal{H}^{(L)}$ is defined by

$$\mathcal{H}^{(L)} = \sum_{\text{helicity}} A_6^{(0)*} F_6^{(L)} \,, \tag{5.5}$$

for all scattering channels given in Eqs. (5.2) and (5.3). The reduced squared finite remainder obeys the same decomposition according to the closed fermion loop contributions as $F_6^{(L)}$,

$$\mathcal{H}^{(1)} = N_c \mathcal{H}^{(1),1} + n_f \mathcal{H}^{(1),n_f} \,,$$
$$\mathcal{H}^{(2)} = N_c^2 \mathcal{H}^{(2),1} + N_c n_f \mathcal{H}^{(2),n_f} + n_f^2 \mathcal{H}^{(2),n_f^2} \,. \tag{5.6}$$

We present a benchmark evaluation at the following phase-space point in the physical scattering region specified by Eq. 5.1 (the momenta are given in units of GeV),

$$
\begin{aligned}
p_1 &= (88.551333054, -22.100690287, 40.080353191, -75.805430956)\,, \\
p_2 &= (-500, 0, 0, -500)\,, \\
p_4 &= (328.32941922, -103.84961188, -301.93375538, 76.494921387)\,, \\
p_2 &= (-500, 0, 0, 500)\,, \\
p_5 &= (152.35810946, -105.88095966, -97.709638326, 49.548385226)\,, \\
p_6 &= (430.76113825, 231.83126183, 359.56304052, -50.237875657)\,,
\end{aligned}
\tag{5.7}
$$

with $\text{tr}_5 = 2.167055i \cdot 10^{10}$ GeV^4. We take the W boson mass and width to be

$$M_W = 80.4109 \text{ GeV}\,, \qquad \Gamma_W = 2.0467 \text{ GeV}\,. \tag{5.8}$$

High precision values for the phase space point in Eq. (5.7) as well as the input parameters in Eq. (5.8) are provided in the ancillary files. We present in Tables 2 and 3 the values of the bare two-loop amplitudes normalised to the tree-level amplitudes in the $\mathbf{u\bar{d}}$ scattering channel for each individual sub-amplitude,

$$\hat{A}_{6,i}^{(L),j} = \frac{A_{6,i}^{(L),j}}{A_{6,i}^{(0)}}\,, \tag{5.9}$$

for $i = u, d, W, e$ and the two closed fermion loop contributions specified in Eq. (2.7), namely $j = 1, n_f$. The results are presented only for the two independent helicity configurations ($+++--+$ and $-++--+$). In Table 4 we show the values of the two-loop reduced squared finite remainders normalised to the reduced squared tree-level amplitudes,

$$\hat{\mathcal{H}}^{(L)} = \frac{\mathcal{H}^{(L)}}{\mathcal{H}^{(0)}}\,, \tag{5.10}$$

for all channels of both $pp \to W^+\gamma j$ and $pp \to W^-\gamma j$ production. We give analogous tables for the one-loop amplitudes in Appendix B.

In order to show the suitability and stability of our evaluation strategy, we present in Figure 3 the evaluation of the reduced squared finite remainders on a one-dimensional slice of

	helicity	ϵ^{-4}	ϵ^{-3}	ϵ^{-2}	ϵ^{-1}	ϵ^{0}
$\hat{A}_{6,u}^{(2),1}$	$+++--+$	2	-49.5288	$603.232 +$ $4.18740i$	$-4813.11 -$ $82.3401i$	$28289.7 +$ $713.980i$
	$-++--+$	2	-49.5288	$605.560 +$ $1.03233i$	$-4867.68 -$ $10.1740i$	$28904.1 -$ $84.4212i$
$\hat{A}_{6,d}^{(2),1}$	$+++--+$	2	-49.5288	$606.017 +$ $4.37613i$	$-4883.27 -$ $87.6955i$	$29148.2 +$ $787.284i$
	$-++--+$	2	-49.5288	$604.589 +$ $4.36093i$	$-4848.83 -$ $90.4281i$	$28743.3 +$ $856.481i$
$\hat{A}_{6,W}^{(2),1}$	$+++--+$	2	-49.5288	$605.100 +$ $3.07126i$	$-4859.29 -$ $58.7793i$	$28844.2 +$ $480.026i$
	$-++--+$	2	-49.5288	$605.637 +$ $2.40762i$	$-4871.59 -$ $43.1992i$	$28978.3 +$ $302.671i$
$\hat{A}_{6,e}^{(2),1}$	$+++--+$	2	-49.5288	$605.140 +$ $2.93702i$	$-4860.19 -$ $55.6437i$	$28853.6 +$ $444.669i$
	$-++--+$	2	-49.5288	$606.606 +$ $2.97710i$	$-4894.35 -$ $56.2398i$	$29236.9 +$ $444.300i$

Table 2: Bare two-loop helicity sub-amplitudes (normalised to the tree-level amplitudes as in Eq. (5.9)) without any closed fermion loop contribution for $W^+\gamma j$ production in the $u\bar{d}$ scattering channel evaluated at the kinematic point given in Eq. (5.7). The results are shown for the two independent helicity configurations and obtained with $q_1 = p_3$ and $q_3 = p_1$ where q_1 (q_3) is the reference momentum for the photon (gluon) polarisation vector.

the physical phase space for all channels of $W^+\gamma j$ production. We begin by parameterising the momenta of the one-mass five-particle process relevant for the W-production amplitudes as

$$
\begin{aligned}
p_1^\mu &= u_1 \frac{\sqrt{s}}{2} \left(1, 1, 0, 0\right) , \\
p_2^\mu &= \frac{\sqrt{s}}{2} \left(-1, 0, 0, -1\right) , \\
p_3^\mu &= u_2 \frac{\sqrt{s}}{2} \left(1, \cos\theta, -\sin\phi \sin\theta, -\cos\phi \sin\theta\right) , \\
p_4^\mu &= \frac{\sqrt{s}}{2} \left(-1, 0, 0, 1\right) .
\end{aligned}
\tag{5.11}
$$

We fix the value of $\cos\theta$ by requiring that

$$
(p_5 + p_6)^2 = M_{ll}^2 ,
\tag{5.12}
$$

where M_{ll}^2 is the invariant mass of the leptonic pair. We then parameterise the momenta

	helicity	ϵ^{-4}	ϵ^{-3}	ϵ^{-2}	ϵ^{-1}	ϵ^{0}
$\hat{A}_{6,u}^{(2),n_f}$	$+++--+$	0	0.333333	-7.39369	$79.8302 +$ $1.39580i$	$-556.215 -$ $14.3791i$
	$-++--+$	0	0.333333	-7.39369	$80.6063 +$ $0.34411i$	$-570.821 +$ $1.89741i$
$\hat{A}_{6,d}^{(2),n_f}$	$+++--+$	0	0.333333	-7.39369	$80.7586 +$ $1.45871i$	$-576.048 -$ $17.8798i$
	$-++--+$	0	0.333333	-7.39369	$80.2827 +$ $1.45364i$	$-566.721 -$ $19.4318i$
$\hat{A}_{6,W}^{(2),n_f}$	$+++--+$	0	0.333333	-7.39369	$80.4531 +$ $1.02375i$	$-569.113 -$ $9.88866i$
	$-++--+$	0	0.333333	-7.39369	$80.6321 +$ $0.802539i$	$-572.278 -$ $6.31448i$
$\hat{A}_{6,e}^{(2),n_f}$	$+++--+$	0	0.333333	-7.39369	$80.4664 +$ $0.979007i$	$-569.368 -$ $9.14880i$
	$-++--+$	0	0.333333	-7.39369	$80.9551 +$ $0.992365i$	$-577.544 -$ $9.72557i$

Table 3: Bare two-loop helicity sub-amplitudes (normalised to the tree-level amplitudes as in Eq. (5.9)) with one closed fermion loop for $W^+\gamma j$ production in the $\mathbf{u\bar{d}}$ scattering channel evaluated at the kinematic point given in Eq. (5.7). The results are shown for the two independent helicity configurations and obtained with $q_1 = p_3$ and $q_3 = p_1$ where q_1 (q_3) is the reference momentum for the photon (gluon) polarisation vector.

of the leptonic pair,

$$p_5^\mu = u_3 \frac{\sqrt{s}}{2} \left(1, \cos\theta_{ll}, -\sin\phi_{ll}\sin\theta_{ll}, -\cos\phi_{ll}\sin\theta_{ll}\right), \qquad (5.13)$$

and p_6 follows from momentum conservation. We fix u_3 by requiring that $p_6^2 = 0$. In order to define a univariate phase-space slice, we choose

$$s = 10^4\,\text{GeV}^2\,, \qquad M_{ll} = 60\,\text{GeV}\,, \qquad \phi = \frac{1}{10}\,, \qquad u_1 = \frac{1}{7}\,, \qquad \theta_{ll} = \frac{\pi}{2}\,, \qquad \phi_{ll} = \frac{\pi}{3}\,. \tag{5.14}$$

The remaining variable, u_2, is constrained to the interval $[87/175, 29/50]$. We chose these values arbitrarily so that the slice crosses a number of spurious poles, i.e. points where the rational coefficients diverge whereas the finite remainders stay finite. We checked explicitly that, while approaching such spurious poles, the values of the rational coefficients become larger and larger, while the finite remainders converge. This is a robust check of the stability of the evaluation, since the convergence requires large numerical cancellations among various terms of the finite remainders. Figure 3 shows the plots of the reduced

$W^+\gamma j$	$\mathrm{Re}\,\hat{\mathcal{H}}^{(2),1}$	$\mathrm{Re}\,\hat{\mathcal{H}}^{(2),n_f}$	$\mathrm{Re}\,\hat{\mathcal{H}}^{(2),n_f^2}$
u$\bar{\mathrm{d}}$	483.506205134	-222.568846475	22.1747738519
$\bar{\mathrm{d}}$u	462.732386147	-219.389809502	22.1747738519
ug	894.669569294	-309.802310098	24.2425489305
gu	796.031872994	-288.292629199	23.3127252902
$\bar{\mathrm{d}}$g	954.097242371	-317.336400774	24.2425489305
g$\bar{\mathrm{d}}$	898.961273740	-302.856612446	23.3127252902
$W^-\gamma j$	$\mathrm{Re}\,\hat{\mathcal{H}}^{(2),1}$	$\mathrm{Re}\,\hat{\mathcal{H}}^{(2),n_f}$	$\mathrm{Re}\,\hat{\mathcal{H}}^{(2),n_f^2}$
d$\bar{\mathrm{u}}$	498.332524932	-222.702160434	22.1747738519
$\bar{\mathrm{u}}$d	732.600496818	-268.121335492	22.1747738519
dg	1786.14253164	-305.863467669	24.2425489305
gd	1612.34790163	-407.732735568	23.3127252902
$\bar{\mathrm{u}}$g	320.710353060	-152.382317276	24.2425489305
g$\bar{\mathrm{u}}$	1300.37372328	-375.944229843	23.3127252902

Table 4: Reduced squared finite remainders (normalised to the reduced squared tree level amplitudes) for all closed fermion loop contributions and scattering channels evaluated at the kinematic point given in Eq. (5.7) for both $pp \to W^+\gamma j$ and $pp \to W^-\gamma j$ production.

squared finite remainders up to two-loop order for all channels of $W^+\gamma j$ production on the univariate phase-space slice defined above.

6 Conclusions

In this article we have presented the two-loop leading colour QCD helicity amplitudes for the process $W^\pm\gamma j$ for the first time. We have obtained relatively compact analytic expressions that can be efficiently evaluated across the full physical phase-space. We constructed the colour and helicity summed finite remainders, and performed several validation tests. This opens the path for precision phenomenological predictions at NNLO accuracy in the strong coupling.

To obtain the best possible theoretical predictions it will be necessary to improve upon the leading colour approximation taken in this article. While it is expected that the leading colour contribution dominates, a quantitative statement is not possible without explicit computation. Sub-leading colour corrections require non-planar topologies to be taken into account, and represent a considerable increase in analytic and algebraic complexity. Progress on the relevant Feynman integrals has been made in this direction quite recently [47], although a few topologies contributing to the full amplitudes are still missing. We note that the missing closed fermion loop contributions, $A_{6,q}^{(2)}$, only require non-planar
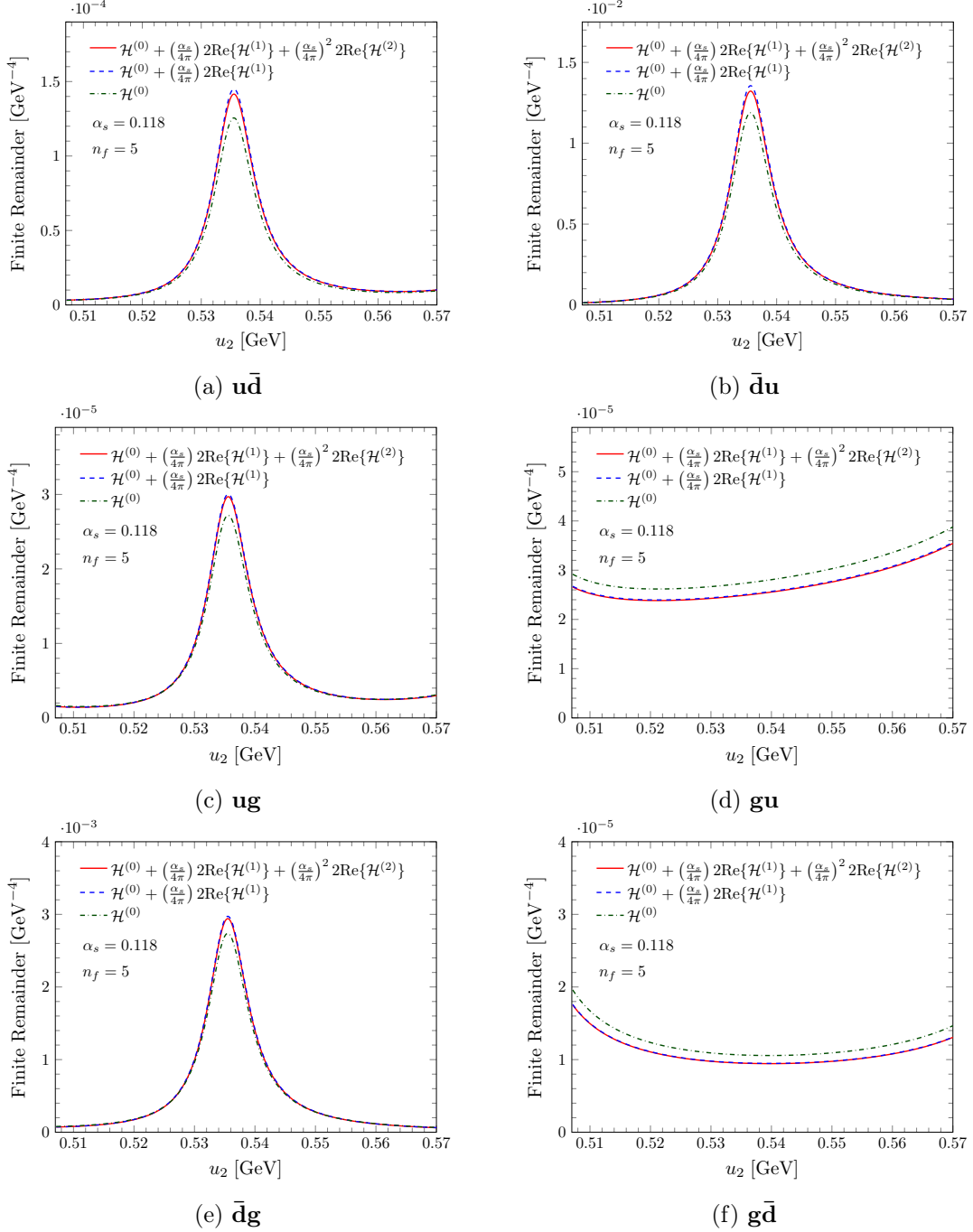
Figure 3: Reduced squared finite remainders $\mathcal{H}^{(L)}$ at tree level, one and two loops evaluated on the univariate phase-space slice defined by Eqs. (5.11), (5.12) and (5.13), with the parameters given in Eq. (5.14), for all channels of $W^+\gamma j$ production defined in Eq. (5.2).

hexaboxes and therefore could be considered on a shorter timescale.

We also hope that our approach to the simplification of the reconstructed amplitudes will be of use in subsequent amplitude computations. An improved understanding of how

a rational parameterisation can be tuned to simplify a particular rational coefficient would certainly be of great value. We expect this to be of particular importance when dealing with sub-leading colour and non-planar configurations, in which many different orderings appear simultaneously. It would also be interesting to study the effect of this method on the reconstruction of the amplitude, i.e. whether the reconstruction is performed in terms of s_{ij}, tr_5 variables or a rational parametrisation.

Acknowledgments

A Renormalisation Constants

In this appendix we list the values of the β function coefficients and anomalous dimensions relevant for the IR and UV structure of the amplitudes discussed in Section 2 [59]:

$$\beta_0 = \frac{11}{3}C_A - \frac{4}{3}T_F n_f\,, \tag{A.1}$$

$$\beta_1 = \frac{34}{3}C_A^2 - \frac{20}{3}C_A T_F n_f - 4C_F T_F n_f\,, \tag{A.2}$$

$$\gamma_0^g = -\frac{11}{3}C_A + \frac{4}{3}T_F n_f\,, \tag{A.3}$$

$$\gamma_1^g = C_A^2\left(-\frac{692}{27} + \frac{11\pi^2}{18} + 2\zeta_3\right) + 4C_F T_F n_f + C_A T_F n_f\left(\frac{256}{27} - \frac{2\pi^2}{9}\right)\,, \tag{A.4}$$

$$\gamma_0^q = -3C_F\,, \tag{A.5}$$

$$\gamma_1^q = C_F^2\left(-\frac{3}{2} + 2\pi^2 - 24\zeta_3\right) + C_F C_A\left(-\frac{961}{54} - \frac{11\pi^2}{6} + 26\zeta_3\right)$$
$$+ C_F T_F n_f\left(\frac{130}{27} + \frac{2\pi^2}{3}\right)\,, \tag{A.6}$$

$$\gamma_0^{\mathrm{cusp}} = 4\,, \tag{A.7}$$

$$\gamma_1^{\mathrm{cusp}} = \left(\frac{268}{9} - \frac{4\pi^2}{3}\right)C_A - \frac{80}{9}T_F n_f\,, \tag{A.8}$$

where $C_A = N_c$, $C_F = (N_c^2 - 1)/(2N_c)$, and $T_F = 1/2$.

B One-Loop Results

We show in Table 5 the numerical values of the one-loop bare sub-amplitudes normalised to the tree-level amplitudes ($\hat{A}_i^{(1),1}$ for $i = u, d, W, e$) in the $\mathbf{u\bar{d}}$ scattering channel evaluated

	helicity	ϵ^{-2}	ϵ^{-1}	ϵ^0	ϵ^1	ϵ^2
$\hat{A}_u^{(1),1}$	$+++--+$	-2	23.8477	$-138.615 - 2.09370i$	$523.949 + 12.3666i$	$-1448.23 - 21.7701i$
	$-++--+$	-2	23.8477	$-139.779 - 0.516164i$	$535.218 - 2.01397i$	$-1503.32 + 46.1044i$
$\hat{A}_d^{(1),1}$	$+++--+$	-2	23.8477	$-140.008 - 2.18806i$	$539.871 + 13.7461i$	$-1538.48 - 30.4669i$
	$-++--+$	-2	23.8477	$-139.294 - 2.18046i$	$532.471 + 15.2170i$	$-1499.51 - 44.3866i$
$\hat{A}_W^{(1),1}$	$+++--+$	-2	23.8477	$-139.550 - 1.53563i$	$534.185 + 8.26368i$	$-1503.99 - 6.62167i$
	$-++--+$	-2	23.8477	$-139.818 - 1.20381i$	$536.639 + 5.03856i$	$-1515.10 + 9.39205i$
$\hat{A}_e^{(1),1}$	$+++--+$	-2	23.8477	$-139.570 - 1.46851i$	$534.360 + 7.61926i$	$-1504.71 - 3.48177i$
	$-++--+$	-2	23.8477	$-140.303 - 1.48855i$	$541.353 + 7.64165i$	$-1538.44 - 2.31498i$

Table 5: Bare one-loop helicity sub-amplitudes (normalised to the tree-level amplitudes as in Eq. (5.9)) without any closed fermion loop contribution for $W^+\gamma j$ production in the $\mathbf{u\bar{d}}$ scattering channel evaluated at the kinematic point given in Eq. (5.7). The results are shown for the two independent helicity configurations and obtained with $q_1 = p_3$ and $q_3 = p_1$ where q_1 (q_3) is the reference momentum for the photon (gluon) polarisation vector.

at the kinematic point given in Eq. (5.7). The corresponding reduced squared tree-level amplitudes $\mathcal{H}^{(0)}$ and reduced squared one-loop finite remainders normalised to the reduced squared tree-level amplitudes ($\hat{\mathcal{H}}^{(1),j}$ with $j = 1, n_f$) are shown in Table 6 for both $W^+\gamma j$ and $W^-\gamma j$ production.

References

[1] CMS collaboration, S. Chatrchyan et al., *Measurement of $W\gamma$ and $Z\gamma$ production in pp collisions at $\sqrt{s} = 7$ TeV*, *Phys. Lett. B* **701** (2011) 535–555, [1105.2758].

[2] ATLAS collaboration, G. Aad et al., *Measurement of Wgamma and Zgamma production in proton-proton collisions at $\sqrt{s} = 7$ TeV with the ATLAS Detector*, *JHEP* **09** (2011) 072, [1106.1592].

[3] ATLAS collaboration, G. Aad et al., *Measurement of $W\gamma$ and $Z\gamma$ production cross sections in pp collisions at $\sqrt{s} = 7$ TeV and limits on anomalous triple gauge couplings with the ATLAS detector*, *Phys. Lett. B* **717** (2012) 49–69, [1205.2531].

$W^+\gamma j$	$\mathcal{H}^{(0)}$ [$\times 10^{-10}$ GeV^{-4}]	Re $\hat{\mathcal{H}}^{(1),1}$	Re $\hat{\mathcal{H}}^{(1),n_f}$
u$\bar{\text{d}}$	32.9224527109	-20.4269208141	4.22462265354
$\bar{\text{d}}$u	35.8863373066	-20.0350027848	4.22462265354
ug	4.84655650134	-26.9389515414	4.45445318051
gu	15.2151742999	-25.3235043118	4.37533965902
$\bar{\text{d}}$g	9.18270882925	-28.3542876136	4.45445318051
g$\bar{\text{d}}$	26.4333120479	-27.3120879601	4.37533965902
$W^-\gamma j$	$\mathcal{H}^{(0)}$ [$\times 10^{-10}$ GeV^{-4}]	Re $\hat{\mathcal{H}}^{(1),1}$	Re $\hat{\mathcal{H}}^{(1),n_f}$
d$\bar{\text{u}}$	48.5521763841	-20.5759435967	4.22462265354
$\bar{\text{u}}$d	5.60724308955	-25.0921274652	4.22462265354
dg	0.161819754065	-53.2745933316	4.45445318051
gd	2.59919214772	-35.7387232774	4.37533965902
$\bar{\text{u}}$g	0.471356750696	-25.5067063821	4.45445318051
g$\bar{\text{u}}$	27.6357549618	-32.8902240077	4.37533965902

Table 6: Reduced squared tree-level amplitude (absolute) and reduced squared one-loop finite remainders (normalised to the reduced squared tree amplitudes) for the various closed fermion loop contributions and scattering channels of both $pp \to W^+\gamma j$ and $pp \to W^-\gamma j$ production, evaluated at the kinematic point given in Eq. (5.7).

[4] ATLAS collaboration, G. Aad et al., *Measurements of $W\gamma$ and $Z\gamma$ production in pp collisions at $\sqrt{s}$=7 TeV with the ATLAS detector at the LHC*, *Phys. Rev. D* **87** (2013) 112003, [1302.1283].

[5] CMS collaboration, S. Chatrchyan et al., *Measurement of the $W\gamma$ and $Z\gamma$ Inclusive Cross Sections in pp Collisions at $\sqrt{s}$ = 7 TeV and Limits on Anomalous Triple Gauge Boson Couplings*, *Phys. Rev. D* **89** (2014) 092005, [1308.6832].

[6] CMS collaboration, A. M. Sirunyan et al., *Measurement of the $W\gamma$ Production Cross Section in Proton-Proton Collisions at $\sqrt{s}$=13 TeV and Constraints on Effective Field Theory Coefficients*, *Phys. Rev. Lett.* **126** (2021) 252002, [2102.02283].

[7] T. Gehrmann and L. Tancredi, *Two-loop QCD helicity amplitudes for $q\bar{q} \to W^{\pm}\gamma$ and $q\bar{q} \to Z^0\gamma$*, *JHEP* **02** (2012) 004, [1112.1531].

[8] M. Grazzini, S. Kallweit and D. Rathlev, *$W\gamma$ and $Z\gamma$ production at the LHC in NNLO QCD*, *JHEP* **07** (2015) 085, [1504.01330].

[9] J. M. Campbell, G. De Laurentis, R. K. Ellis and S. Seth, *The $pp \to W(\to l\nu) + \gamma$ process at next-to-next-to-leading order*, *JHEP* **07** (2021) 079, [2105.00954].

[10] E. Accomando, A. Denner and C. Meier, *Electroweak corrections to $W\gamma$ and $Z\gamma$ production at the LHC*, *Eur. Phys. J. C* **47** (2006) 125–146, [hep-ph/0509234].

[11] A. Denner, S. Dittmaier, M. Hecht and C. Pasold, *NLO QCD and electroweak corrections to*

$W + \gamma$ *production with leptonic W-boson decays*, *JHEP* **04** (2015) 018, [1412.7421].

[12] M. Grazzini, S. Kallweit, J. M. Lindert, S. Pozzorini and M. Wiesemann, *NNLO QCD + NLO EW with Matrix+OpenLoops: precise predictions for vector-boson pair production*, *JHEP* **02** (2020) 087, [1912.00068].

[13] S. Catani and M. Grazzini, *An NNLO subtraction formalism in hadron collisions and its application to Higgs boson production at the LHC*, *Phys. Rev. Lett.* **98** (2007) 222002, [hep-ph/0703012].

[14] R. Boughezal, C. Focke, W. Giele, X. Liu and F. Petriello, *Higgs boson production in association with a jet at NNLO using jettiness subtraction*, *Phys. Lett. B* **748** (2015) 5–8, [1505.03893].

[15] J. Gaunt, M. Stahlhofen, F. J. Tackmann and J. R. Walsh, *N-jettiness Subtractions for NNLO QCD Calculations*, *JHEP* **09** (2015) 058, [1505.04794].

[16] M. Grazzini, S. Kallweit and M. Wiesemann, *Fully differential NNLO computations with MATRIX*, *Eur. Phys. J. C* **78** (2018) 537, [1711.06631].

[17] R. Boughezal, J. M. Campbell, R. K. Ellis, C. Focke, W. Giele, X. Liu et al., *Color singlet production at NNLO in MCFM*, *Eur. Phys. J. C* **77** (2017) 7, [1605.08011].

[18] T. Cridge, M. A. Lim and R. Nagar, *Wγ production at NNLO+PS accuracy in GENEVA*, 2105.13214.

[19] CMS collaboration, A. Tumasyan et al., *Measurement of $W^{\pm}\gamma$ differential cross sections in proton-proton collisions at $\sqrt{s} = 13$ TeV and effective field theory constraints*, 2111.13948.

[20] F. Campanario, C. Englert, M. Spannowsky and D. Zeppenfeld, *NLO-QCD corrections to Wγj production*, *EPL* **88** (2009) 11001, [0908.1638].

[21] F. Campanario, C. Englert and M. Spannowsky, *Precise predictions for (non-standard) Wγ + jet production*, *Phys. Rev. D* **83** (2011) 074009, [1010.1291].

[22] T. Gehrmann, J. Henn and N. Lo Presti, *Analytic form of the two-loop planar five-gluon all-plus-helicity amplitude in QCD*, *Phys. Rev. Lett.* **116** (2016) 062001, [1511.05409].

[23] S. Badger, C. Brønnum-Hansen, H. B. Hartanto and T. Peraro, *Analytic helicity amplitudes for two-loop five-gluon scattering: the single-minus case*, *JHEP* **01** (2019) 186, [1811.11699].

[24] S. Abreu, L. J. Dixon, E. Herrmann, B. Page and M. Zeng, *The two-loop five-point amplitude in $\mathcal{N} = 4$ super-Yang-Mills theory*, *Phys. Rev. Lett.* **122** (2019) 121603, [1812.08941].

[25] D. Chicherin, T. Gehrmann, J. Henn, P. Wasser, Y. Zhang and S. Zoia, *Analytic result for a two-loop five-particle amplitude*, *Phys. Rev. Lett.* **122** (2019) 121602, [1812.11057].

[26] D. Chicherin, T. Gehrmann, J. M. Henn, P. Wasser, Y. Zhang and S. Zoia, *The two-loop five-particle amplitude in $\mathcal{N} = 8$ supergravity*, *JHEP* **03** (2019) 115, [1901.05932].

[27] S. Abreu, L. J. Dixon, E. Herrmann, B. Page and M. Zeng, *The two-loop five-point amplitude in $\mathcal{N} = 8$ supergravity*, *JHEP* **03** (2019) 123, [1901.08563].

[28] S. Abreu, J. Dormans, F. Febres Cordero, H. Ita and B. Page, *Analytic Form of Planar Two-Loop Five-Gluon Scattering Amplitudes in QCD*, *Phys. Rev. Lett.* **122** (2019) 082002, [1812.04586].

[29] S. Abreu, F. Febres Cordero, H. Ita, B. Page and V. Sotnikov, *Planar Two-Loop Five-Parton Amplitudes from Numerical Unitarity*, *JHEP* **11** (2018) 116, [1809.09067].

[30] S. Abreu, J. Dormans, F. Febres Cordero, H. Ita, B. Page and V. Sotnikov, *Analytic Form of the Planar Two-Loop Five-Parton Scattering Amplitudes in QCD*, *JHEP* **05** (2019) 084, [1904.00945].

[31] S. Badger, D. Chicherin, T. Gehrmann, G. Heinrich, J. Henn, T. Peraro et al., *Analytic form of the full two-loop five-gluon all-plus helicity amplitude*, *Phys. Rev. Lett.* **123** (2019) 071601, [1905.03733].

[32] S. Abreu, B. Page, E. Pascual and V. Sotnikov, *Leading-Color Two-Loop QCD Corrections for Three-Photon Production at Hadron Colliders*, *JHEP* **01** (2021) 078, [2010.15834].

[33] H. A. Chawdhry, M. Czakon, A. Mitov and R. Poncelet, *Two-loop leading-color helicity amplitudes for three-photon production at the LHC*, *JHEP* **06** (2021) 150, [2012.13553].

[34] S. Caron-Huot, D. Chicherin, J. Henn, Y. Zhang and S. Zoia, *Multi-Regge Limit of the Two-Loop Five-Point Amplitudes in $\mathcal{N}=4$ Super Yang-Mills and $\mathcal{N}=8$ Supergravity*, *JHEP* **10** (2020) 188, [2003.03120].

[35] D. Chicherin and V. Sotnikov, *Pentagon Functions for Scattering of Five Massless Particles*, *JHEP* **12** (2020) 167, [2009.07803].

[36] G. De Laurentis and D. Maître, *Two-Loop Five-Parton Leading-Colour Finite Remainders in the Spinor-Helicity Formalism*, *JHEP* **02** (2021) 016, [2010.14525].

[37] B. Agarwal, F. Buccioni, A. von Manteuffel and L. Tancredi, *Two-loop leading colour QCD corrections to $q\bar{q} \to \gamma\gamma g$ and $qg \to \gamma\gamma q$*, *JHEP* **04** (2021) 201, [2102.01820].

[38] S. Abreu, F. F. Cordero, H. Ita, B. Page and V. Sotnikov, *Leading-color two-loop QCD corrections for three-jet production at hadron colliders*, *JHEP* **07** (2021) 095, [2102.13609].

[39] H. A. Chawdhry, M. Czakon, A. Mitov and R. Poncelet, *Two-loop leading-colour QCD helicity amplitudes for two-photon plus jet production at the LHC*, *JHEP* **07** (2021) 164, [2103.04319].

[40] B. Agarwal, F. Buccioni, A. von Manteuffel and L. Tancredi, *Two-Loop Helicity Amplitudes for Diphoton Plus Jet Production in Full Color*, *Phys. Rev. Lett.* **127** (2021) 262001, [2105.04585].

[41] S. Badger, C. Brønnum-Hansen, D. Chicherin, T. Gehrmann, H. B. Hartanto, J. Henn et al., *Virtual QCD corrections to gluon-initiated diphoton plus jet production at hadron colliders*, *JHEP* **11** (2021) 083, [2106.08664].

[42] S. Badger, H. B. Hartanto and S. Zoia, *Two-Loop QCD Corrections to $Wb\bar{b}$ Production at Hadron Colliders*, *Phys. Rev. Lett.* **127** (2021) 012001, [2102.02516].

[43] S. Badger, H. B. Hartanto, J. Kryś and S. Zoia, *Two-loop leading-colour QCD helicity amplitudes for Higgs boson production in association with a bottom-quark pair at the LHC*, *JHEP* **11** (2021) 012, [2107.14733].

[44] S. Abreu, F. F. Cordero, H. Ita, M. Klinkert, B. Page and V. Sotnikov, *Leading-Color Two-Loop Amplitudes for Four Partons and a W Boson in QCD*, 2110.07541.

[45] C. G. Papadopoulos, D. Tommasini and C. Wever, *The Pentabox Master Integrals with the Simplified Differential Equations approach*, *JHEP* **04** (2016) 078, [1511.09404].

[46] C. G. Papadopoulos and C. Wever, *Internal Reduction method for computing Feynman Integrals*, *JHEP* **02** (2020) 112, [1910.06275].

[47] S. Abreu, H. Ita, B. Page and W. Tschernow, *Two-Loop Hexa-Box Integrals for Non-Planar Five-Point One-Mass Processes*, 2107.14180.

[48] S. Abreu, H. Ita, F. Moriello, B. Page, W. Tschernow and M. Zeng, *Two-Loop Integrals for Planar Five-Point One-Mass Processes*, *JHEP* **11** (2020) 117, [2005.04195].

[49] D. D. Canko, C. G. Papadopoulos and N. Syrrakos, *Analytic representation of all planar two-loop five-point Master Integrals with one off-shell leg*, *JHEP* **01** (2021) 199, [2009.13917].

[50] N. Syrrakos, *Pentagon integrals to arbitrary order in the dimensional regulator*, *JHEP* **06** (2021) 037, [2012.10635].

[51] D. Chicherin, V. Sotnikov and S. Zoia, *Pentagon Functions for One-Mass Planar Scattering Amplitudes*, 2110.10111.

[52] A. von Manteuffel and R. M. Schabinger, *A novel approach to integration by parts reduction*, *Phys. Lett. B* **744** (2015) 101–104, [1406.4513].

[53] T. Peraro, *Scattering amplitudes over finite fields and multivariate functional reconstruction*, *JHEP* **12** (2016) 030, [1608.01902].

[54] T. Peraro, *FiniteFlow: multivariate functional reconstruction using finite fields and dataflow graphs*, *JHEP* **07** (2019) 031, [1905.08019].

[55] F. V. Tkachov, *A Theorem on Analytical Calculability of Four Loop Renormalization Group Functions*, *Phys. Lett.* **100B** (1981) 65–68.

[56] K. G. Chetyrkin and F. V. Tkachov, *Integration by Parts: The Algorithm to Calculate β Functions in 4 Loops*, *Nucl. Phys.* **B192** (1981) 159–204.

[57] S. Laporta, *High precision calculation of multiloop Feynman integrals by difference equations*, *Int. J. Mod. Phys. A* **15** (2000) 5087–5159, [hep-ph/0102033].

[58] S. Catani, *The Singular behavior of QCD amplitudes at two loop order*, *Phys. Lett.* **B427** (1998) 161–171, [hep-ph/9802439].

[59] T. Becher and M. Neubert, *On the Structure of Infrared Singularities of Gauge-Theory Amplitudes*, *JHEP* **06** (2009) 081, [0903.1126].

[60] T. Becher and M. Neubert, *Infrared singularities of scattering amplitudes in perturbative QCD*, *Phys. Rev. Lett.* **102** (2009) 162001, [0901.0722].

[61] E. Gardi and L. Magnea, *Factorization constraints for soft anomalous dimensions in QCD scattering amplitudes*, *JHEP* **03** (2009) 079, [0901.1091].

[62] T. Peraro and L. Tancredi, *Physical projectors for multi-leg helicity amplitudes*, *JHEP* **07** (2019) 114, [1906.03298].

[63] T. Peraro and L. Tancredi, *Tensor decomposition for bosonic and fermionic scattering amplitudes*, *Phys. Rev. D* **103** (2021) 054042, [2012.00820].

[64] A. Hodges, *Eliminating spurious poles from gauge-theoretic amplitudes*, *JHEP* **05** (2013) 135, [0905.1473].

[65] S. Badger, H. Frellesvig and Y. Zhang, *A Two-Loop Five-Gluon Helicity Amplitude in QCD*, *JHEP* **12** (2013) 045, [1310.1051].

[66] S. Badger, *Automating QCD amplitudes with on-shell methods*, *J. Phys. Conf. Ser.* **762** (2016) 012057, [1605.02172].

[67] L. W. Garland, T. Gehrmann, E. W. N. Glover, A. Koukoutsakis and E. Remiddi, *Two loop QCD helicity amplitudes for* $e^+e^- \to$ *three jets*, *Nucl. Phys. B* **642** (2002) 227–262, [hep-ph/0206067].

[68] S. Badger, E. Chaubey, H. B. Hartanto and R. Marzucca, *Two-loop leading colour QCD helicity amplitudes for top quark pair production in the gluon fusion channel*, *JHEP* **06** (2021) 163, [2102.13450].

[69] P. Nogueira, *Automatic Feynman graph generation*, *J. Comput. Phys.* **105** (1993) 279–289.

[70] J. Kuipers, T. Ueda, J. A. M. Vermaseren and J. Vollinga, *FORM version 4.0*, *Comput. Phys. Commun.* **184** (2013) 1453–1467, [1203.6543].

[71] B. Ruijl, T. Ueda and J. Vermaseren, *FORM version 4.2*, 1707.06453.

[72] R. N. Lee, *Presenting LiteRed: a tool for the Loop InTEgrals REDuction*, 1212.2685.

[73] L. E. K., *Factorization of rational functions of several variables into partial fractions*, *Izvestiya Vysshikh Uchebnykh Zavedenii. Matematika* **47** (1978) .

[74] A. Raichev, *Leinartas's partial fraction decomposition*, *arXiv e-prints* (June, 2012) arXiv:1206.4740, [1206.4740].

[75] J. Boehm, M. Wittmann, Z. Wu, Y. Xu and Y. Zhang, *IBP reduction coefficients made simple*, *JHEP* **12** (2020) 054, [2008.13194].

[76] M. Heller and A. von Manteuffel, *MultivariateApart: Generalized partial fractions*, *Comput. Phys. Commun.* **271** (2022) 108174, [2101.08283].

[77] D. Bendle, J. Boehm, M. Heymann, R. Ma, M. Rahn, L. Ristau et al., *Two-loop five-point integration-by-parts relations in a usable form*, 2104.06866.

[78] W. Decker, G.-M. Greuel, G. Pfister and H. Schönemann, "Singular 4-2-1 — A computer algebra system for polynomial computations." http://www.singular.uni-kl.de, 2021.

[79] F. Moriello, *Generalised power series expansions for the elliptic planar families of Higgs + jet production at two loops*, *JHEP* **01** (2020) 150, [1907.13234].

[80] M. Hidding, *DiffExp, a Mathematica package for computing Feynman integrals in terms of one-dimensional series expansions*, *Comput. Phys. Commun.* **269** (2021) 108125, [2006.05510].

[81] H. B. Hartanto, S. Badger, C. Brønnum-Hansen and T. Peraro, *A numerical evaluation of planar two-loop helicity amplitudes for a W-boson plus four partons*, *JHEP* **09** (2019) 119, [1906.11862].

[82] J. Alwall, R. Frederix, S. Frixione, V. Hirschi, F. Maltoni, O. Mattelaer et al., *The automated computation of tree-level and next-to-leading order differential cross sections, and their matching to parton shower simulations*, *JHEP* **07** (2014) 079, [1405.0301].

[83] D. Chicherin, J. M. Henn and G. Papathanasiou, *Cluster algebras for Feynman integrals*, *Phys. Rev. Lett.* **126** (2021) 091603, [2012.12285].